UNIVERSIDADE DE LISBOA

FACULDADE DE CIÊNCIAS

DEPARTAMENTO DE MATEMÁTICA

Coupled Wiener processes: from single to collective dynamics of active particles

Raquel Maria Vicente Filipe

Mestrado em Matemática

Dissertação orientada por:
Professor Doutor Nuno Araújo
Professor Doutor Jean-Claude Zambrini

2017

”The computer must be your slave
and not the opposite.”

Prof. Nuno Araújo

Acknowledgements

I would like to thank my supervisor Prof. Nuno Araújo who introduced me to this exciting topic. I am also grateful to him for all of his availability and support during these past two years in the masters and for all of his kind advice. His editing contributions were extremely valuable for the completion of this thesis.

I would like to thank my co-supervisor Prof. Jean-Claude Zambrini for all his availability and constructive suggestions which were determinant in the realization of this thesis.

I am thankful to the Biomathematics group from CMAF-CIO for all of their contributions and for inviting me to go to an international conference to present about this amazing topic, it was a great experience.

I am very thankful to Prof. Cristóvão Dias from Centro de Física Teórica e Computacional (CFTC) who taught me how to use the High Performance Computing from FCUL to perform the largest simulations of which the results are presented here. Also thanks to him for introducing me to the POV-RAY software and for teaching me how to create images and videos with it.

Thanks to the CFTC group for all the discussions and suggestions for this thesis during the meetings.

I am very thankful to my colleague and friend Bernardo Fernandes for all of his support.

And then I would like to thank my family, in particular, my parents and Francis for all of their support during the development of this thesis. Also, a special thanks to Francis who did an English review of this thesis.

Abstract

Our goal is to study the singular and collective dynamics of active particles and compare them with passive Brownian particle dynamics. We introduce the Wiener process (also known as Brownian motion) and stochastic differential equations after which we present the numerical method used here: the Euler-Maruyama method. The concepts of both passive Brownian particles and active particles are explained and we introduce the concept of drift velocity. We then study the influence of a wall in these dynamics, calculating the probability density function when we consider different conditions such as different total simulation times, different values of drift velocity and different fluids. The existence of two distinct potentials is also considered: one that is purely repulsive and the Lennard-Jones potential, which is attractive and repulsive. Again, we calculate the probability density function in a system with several particles and study cases with different total simulation times and differing values of drift velocity. We consider a two-dimensional system for our conclusions and circular shaped particles.

When comparing the motion of a singular particle, we can conclude that passive Brownian particles show a purely diffusive behaviour, *i.e.* the mean square displacement is linear over time, and active particles show a diffusive behaviour for longer times, *i.e.* times longer than the inverse of the rotational diffusion coefficient, whereas for shorter times, *i.e.* times shorter than the inverse of the rotational diffusion coefficient, they show a ballistic behaviour, *i.e.* the mean square displacement shows a quadratic dependence of time. If we assume the existence of a wall in our system, we notice that the probability density function increases near the walls when fixing the value of drift velocity, while it converges to zero in the remaining regions. Physically, this means that there is an accumulation of particles near the wall since they stay there hitting the wall until their velocity direction changes. We also conclude that for passive Brownian particles, there is a convergence of the probability density function from a normal to a uniform distribution. However, when we consider active particles, the probability density function increases near the wall and it converges to zero in the remaining regions over time. We conclude that this occurs more rapidly as the value of drift velocity increases. When comparing different fluids, *i.e.* fluids with distinct values of translational diffusion coefficient (and so distinct values of rotational diffusion coefficient), we conclude that, for passive Brownian particles, the curve of distribution representing the probability density function becomes wider when the translational diffusion coefficient is larger when keeping the time fixed while, if we vary the time, this curve will be wider over time. For active particles, we concluded that the probability density function increases near the walls over time for a smaller translational diffusion coefficient. For a fixed time of simulation, the larger the value of drift velocity is, the higher the probability density function will be near the walls, which also increases when the translational diffusion coefficient is lowered.

If we assume a repulsive potential between two passive Brownian particles tangent to each other, we conclude that they move away from each other. When we consider two active particles, they move away until they are outside the interaction range of the repulsive potential and then the distance between them stays approximately stable. If we consider several particles, again, we see that, for passive Brownian

particles, there is a convergence of the probability density function to a uniform distribution. When considering active particles, the probability density function increases near the wall over time and it converges to zero in the remaining regions. When increasing the value of drift velocity this occurs faster than if we were considering a smaller value of drift velocity. When considering the Lennard-Jones potential between two particles tangent to each other, the conclusions are the same as for the repulsive potential. In our work we observed that when the depth of the potential well converges to zero, there is a weaker attraction between the particles, which leads to a non-aggregation state. In the opposite case, in which the depth of the potential well is much larger than one, the aggregation between the particles is very strong. This last result does not depend on the value of the drift velocity. When considering several particles, we conclude the same for the probability density function as in the repulsive potential case. For passive Brownian particles, the process of converging to a uniform distribution is slower when considering the purely repulsive potential than the Lennard-Jones potential. For active particles, the process of accumulation of particles near the wall is faster when the repulsive potential is considered than with the Lennard-Jones potential.

Keywords: Wiener process (Brownian motion), stochastic differential equations, active particles.

Resumo

Atualmente é possível observar um crescente desenvolvimento da tecnologia e, nomeadamente, de robots. Cientistas e engenheiros estão a trabalhar com escalas cada vez mais pequenas, como a micro- e a nano-escala. A sociedade pode beneficiar destes desenvolvimentos de diversos modos, como por exemplo, na área da Saúde. Pensemos então na possibilidade de construir micro-robots que são capazes de levar substâncias específicas, como medicamentos, a partes do corpo humano em necessidade [1]. Esta tarefa parece fácil se pensarmos nos mais recentes desenvolvimentos de robots à escala humana, mas o desafio está no facto de que os micro-robots sofrem muitas colisões provenientes do meio em que estão, devido a flutuações térmicas. Tendo este facto em conta, a descrição matemática destas partículas usando teorias da Mecânica torna-se um desafio. Para estudar o movimento dessas partículas, baseamo-nos no movimento de partículas criadas pela Natureza, como por exemplo, um espermatozoide. O seu movimento não é apenas aleatório pois é claro que existe uma direção preferencial de velocidade, à qual chamamos velocidade de deriva. Este termo de velocidade de deriva diz-nos se a partícula é ativa ou não, sendo então uma partícula Browniana passiva. Para descrever as equações de movimento desta partícula, utiliza-se o conceito de processo de Wiener que também é denominado por movimento Browniano. Reduz-se então um problema de vários corpos a um problema de um corpo e para isso é necessário incluir conceitos de Cálculo Estocástico [7], cujo fator principal é o processo de Wiener, e o resultado será uma equação diferencial estocástica como equação de movimento da partícula em estudo. Apesar disso, note-se que não é possível aplicar esta redução a todos os sistemas, pois é necessário preencher os requisitos apropriados, por exemplo esta redução é aplicada quando há interesse em estudar as propriedades globais do sistema e/ou o comportamento mecânico em vez da estrutura molecular e/ou interações químicas ou quando se pretende fazer um estudo simples dos resultados das simulações e do comportamento do sistema. Com esta redução obtêm-se cálculos computacionalmente mais económicos e, além disso, é possível simular sistemas maiores, assim como maiores escalas de tempo, o que permite usar um incremento de tempo maior. Contudo, é importante garantir que os modelos simplificados são capazes de reproduzir as propriedades físicas relevantes.

Utilizando esta equação diferencial estocástica, é possível realizar simulações e explorar várias possibilidades tais como diferentes valores da velocidade de deriva, diferentes tempos totais de simulação, diferentes viscosidades do fluído, introduzir obstáculos (como por exemplo uma parede) e diferentes potenciais de interação entre as partículas.

Para integrar numericamente as equações de movimento, implementou-se o método de Euler-Maruyama [8, 9]. Este método baseia-se no tão conhecido método de Euler que é utilizado para resolver equações diferenciais ordinárias numericamente.

Considerou-se um sistema de duas dimensões e partículas de forma circular. Foram feitas simulações com partículas Brownianas passivas a partículas ativas considerando condições periódicas de fronteira de onde se concluiu que as partículas Brownianas passivas possuem um comportamento puramente difusivo ao longo do tempo, ou seja o deslocamento quadrático médio varia linearmente com o tempo, enquanto

que as partículas ativas possuem um comportamento balístico, ou seja o deslocamento quadrático médio varia quadraticamente com o tempo, para tempos menores do que o inverso do coeficiente de difusão rotacional e comportamento difusivo para tempos maiores do que este.

Nas simulações seguintes considerou-se a presença de uma caixa quadrada no sistema e partículas com a mesma posição inicial. Estas simulações foram realizadas para proceder ao estudo da função densidade de probabilidade. Aqui, para além de termos estudado o impacto de se considerar diferentes valores da velocidade de deriva e diferentes tempos totais de simulação, também se considerou o impacto de um fluido diferente. Observou-se que, no caso das partículas Brownianas passivas, a função densidade de probabilidade convergiu de uma distribuição normal para uma distribuição uniforme ao longo do tempo. No caso das partículas ativas, observou-se que a função densidade de probabilidade aumentou nas regiões próximas das paredes e que diminui nas restantes regiões. Para um tempo fixo e variando a velocidade de deriva das partículas ativas, observou-se o mesmo. Foi possível concluir que, com a presença de paredes, as partículas ativas acumulam-se perto destas e a velocidade deste processo depende do tempo total de simulação e/ou da velocidade de deriva. Este resultado era esperado pois é sabido da teoria que quando uma partícula ativa interage com uma parede, existe uma assimetria entre o movimento de chegada e o de partida da parede. Quando a partícula se aproxima da parede irá ficar próxima da parede até que a orientação da sua velocidade se altere para uma orientação oposta à parede e aí a partícula irá nadar para longe da parede. Esta assimetria faz com que exista uma tendência de acumulação de partículas ativas próximo das paredes. O estudo da acumulação de partículas ativas nas paredes é importante em aplicações, por exemplo no caso em que se supõe que um micro-robot leva uma dada substância a partes específicas do corpo humano, estes robots podem ter tendência a acumular próximos de superfícies no corpo o que pode resultar em elevadas concentrações da substância em questão em locais desejáveis ou não podendo haver, portanto, efeitos secundários indesejáveis.

Ao variar o coeficiente de difusão translacional, observaram-se várias dependências entre o coeficiente de difusão translacional e a velocidade de deriva e também entre o coeficiente de difusão translacional e o tempo total de simulação. Nas simulações com partículas Brownianas passivas observou-se que, fixando o tempo de simulação, ao aumentar o coeficiente de difusão translacional a curva da função densidade de probabilidade era mais larga. Ao longo do tempo, para qualquer coeficiente de difusão translacional estudado, observou-se que a função densidade de probabilidade tornou-se mais larga. No caso com partículas ativas e com variação do coeficiente de difusão translacional, foram observadas as mesmas diferenças de comportamento em relação às partículas Brownianas passivas aquando a introdução das paredes: ao aumentar a velocidade de deriva nos quatro casos de diferente coeficiente de difusão translacional observou-se que o processo de acumulação de partículas próxima da parede era mais rápido. Para um valor de velocidade de deriva fixado, observou-se que a função densidade de probabilidade aumenta próximo das paredes ao longo do tempo nos quatro casos de diferente coeficiente de difusão translacional considerados.

Por fim, consideraram-se interações entre partículas de modo a melhor entender o movimento coletivo de partículas, para isso estudou-se o caso com um potencial puramente repulsivo e com um potencial repulsivo e atrativo (potencial de Lennard-Jones). O primeiro caso estudado foi com duas partículas tangentes uma à outra no início das simulações. No caso com partículas Brownianas passivas, observou-se que, com qualquer dos potenciais considerados, as partículas repelem-se e afastam-se uma da outra. O mesmo acontece com partículas ativas apesar de que após um certo tempo a distância entre elas fica aproximadamente estável. De seguida, ainda considerando os potenciais, estudou-se um sistema com muitas partículas para se estudar a função densidade de probabilidade para diferentes valores da velocidade de deriva e do tempo total de simulação. Aqui observou-se o mesmo comportamento do que

no caso em que as simulações realizadas sem se considerar potencial referido anteriormente: a função densidade de probabilidade no caso de partículas Brownianas passivas converge para uma distribuição uniforme e no caso com partículas ativas, a função densidade de probabilidade atinge valores mais elevados próxima das paredes ao longo do tempo e este processo, mais uma vez, ocorre de modo mais rápido quando se consideram valores da velocidade de deriva mais elevados. No entanto, foram observadas algumas diferenças entre ambos os potenciais: as partículas Brownianas passivas, ao considerar o potencial puramente repulsivo, necessitam de mais tempo até que se distribuam uniformemente pelo espaço e, portanto, exige-se mais tempo até que a função densidade de probabilidade convirja para uma distribuição uniforme; as partículas ativas acumulam-se mais depressa junto das paredes quando se considera o potencial puramente repulsivo do que o potencial de Lennard-Jones.

Existem questões interessantes e importantes em termos de aplicações a serem estudadas no futuro. Por exemplo, se se considerar a existência de obstáculos no fluido [1] será um caso interessante de se estudar o comportamento das partículas ativas e a sua acumulação, por exemplo, para diferentes geometrias do obstáculo. Outra questão interessante será o movimento ativo quiral no qual as partículas ativas nadam em trajetórias circulares [1]. A existência de mais conhecimento científico nestes tópicos irá permitir um maior controle sobre partículas ativas, em particular, partículas ativas criadas pelo Homem tais como os micro- e nano-robots mencionados atrás.

Palavras-chave: Processo de Wiener (movimento Browniano), equações diferenciais estocásticas, partículas ativas.

Contents

List of Figures

Nomenclature

$\langle x \rangle$	Average of x with respect to the distribution of the realizations of the stochastic variable $\xi(t)$
$\mathbb{E}[x]$	Mean of the random variable x
$\mathbb{R}_0^+$	Union of real positive numbers and zero
$\varphi(t)$	Angle between the x-axis and the thrust direction at instant t
$\vec{r}(t)$	position of the Brownian particle at time t; $\vec{r}(t) := (r_x(t), r_y(t), r_z(t))$
$\vec{u}_x$	Versor of the x-axis
$\vec{u}_y$	Versor of the y-axis
$\vec{u}_z$	Versor of the z-axis
d	Spatial dimension, *i.e.* $d \in \{1,2,3\}$
D_R	Rotational diffusion coefficient
D_T	Translational diffusion coefficient
$log(x)$	Natural logarithm of x
v_{drift}	Absolute value of thrust velocity or drift velocity

Chapter 1

Introduction

These days, we live in an age of ever-increasing technology development and we are starting to witness the proliferation of robots within our society. The scales at which scientists and engineers are working are becoming smaller (such as micro and nanoscale). These developments can benefit society in a multitude of ways including, e.g., health protection. What if we had micro-robots that were able to, for example, bring specific substances to targeted parts of our body in need of them [1]? This seems like a relatively straightforward task if you observe all the recent developments on robots at the human scale, but micro-robots are affected by multiple collisions with particles in the surrounding medium, due to thermal fluctuations. If we take that into account, the mathematical description of the motion of these particles using theories (equations of motion) from Mechanics is a challenge, as we will explain here.

In order to study the motion of these particles, we base ourselves in the motion of particles created by Nature, e.g., a spermatozoon. Its motion is not just random since we can notice the existence of a preferred direction of velocity, which we call drift velocity. This term of drift velocity will tell us if the particle is an active particle or not, *i.e.* a passive Brownian particle. To describe the equations of motion of this particle, we use the concept of Wiener process also known as Brownian Motion. We reduce the problem from a many-body problem to a single-body problem and to do so we need to include concepts from Stochastic Calculus [7], whose building block is Wiener process, and the result will be a stochastic differential equation as equation of motion of our particle. We should remark that this reduction cannot be applied to every system since it should meet the appropriate requirements, e.g. we use this reduction when we are interested in studying the global properties of the system and/or mechanical behaviour instead the molecular structure and/or chemical interactions or when we want to do a direct simplified analysis of simulation results and the behaviour of the system. When we do this reduction, we obtain less demanding calculations in terms of computational resources. Moreover, this reduction allows us to access larger systems and longer time scales, it allows us to use larger time step increments (and so larger time scales). However, it is important to guarantee that the simplified models still grasp the relevant physics. With this stochastic differential equation we can perform simulations and then explore many different possibilities such as different values of drift velocity, different total simulation times, different viscosities of the suspending medium, introduce obstacles (e.g. a wall) and different potentials of interaction between the particles.

To integrate the equations of motion, we implemented the Euler-Maruyama Method [8, 9] which is used to solve numerically stochastic differential equations. This method is based on the well-known Euler Method which is used to solve ordinary differential equations numerically.

The thesis is organized as follows: in Chapter 2, we give a short theoretical introduction and we define important concepts from Stochastic Calculus. We also explain the numerical method, Euler-Maruyama

Method, which we will use to integrate our stochastic differential equations. In Chapter 3, we discuss the limit of passive Brownian particles. We also introduce the Langevin approach and explain its importance, which will provide us with answer to the question of why it is not feasible to obtain a deterministic mathematical description of the particle using classical equations of motion known from Mechanics. Then, we do some important deductions that were used in our work. In Chapter 4, we introduce the self-propelled active particle. We explain what they are and the mathematical and physical difference between such a particle and passive Brownian particles. We also give some examples from the real world of this kind of particle to reinforce the importance of thinking about its mathematical description. Then we give a description of the coupled stochastic differential equations which describe the motion of an active particle. In Chapter 5, we present a general framework of passive Brownian and active particles. We present a general summary of the theory of the system of coupled equations and then we explain their numerical implementation. Then we present a short note about random number generators which is something important to consider when we work with simulations with random numbers. In Chapter 6, we introduce the presence of a wall. We consider non-interacting particles with the same initial position and we perform simulations to calculate the probability density function of particle positions. We also study what happens for different values of drift velocity and different simulation times. We also study four different fluids: olive oil, blood at 37^{o}C, water at 20^{o}C and 100^{o}. Again, we analyse what happens for different values of drift velocity and different total simulation time and we do a comparison between the fluids and their impact in the motion of the particles. In Chapter 7, we consider a non-zero potential between the particles (one repulsive and another repulsive and attractive) and we consider particles with different initial position. We simulate two particles to analyse the effect of the potential. We consider a system with several particles to study the probability density function for different values of drift velocity and total simulation time. Finally, in Chapter 8 we draw some conclusions.

Chapter 2

A short theoretical introduction and its numerical implementation

In this chapter we provide a short introduction to the theory of Stochastic Calculus and we describe the numerical implementation that we used to obtain numerical solutions to the equations.

2.1 Theory

As the title suggests, we are going to talk about coupled Wiener processes, but what exactly is a Wiener process?

We should first start with the definition of this process, for which we will follow reference [7] as well as for Definitions 2.2 and 2.3.

Definition 2.1. A **Wiener process**, $W := W(t)$ where $t \geq 0$, is a stationary stochastic process satisfying the following properties:

1. $W(0) = 0$ almost surely;
2. W has independent increments, *i.e.*, $\forall t > 0$ the processes $W(t+u) - W(t)$ $(u \geq 0)$ are independent of $W(s)$ where $s \leq t$;
3. W has Gaussian increments, *i.e.*, $W(t+u) - W(t)$ is normally distributed with mean 0 and variance u;
4. W has continuous paths, *i.e.*, $W(t)$ is continuous in t.

This process is also called **Brownian Motion** due to its historic origin, as we will discuss later. Through this work both denominations will be used: Wiener Process and Brownian Motion.

As we will see, this process plays a fundamental role in the Theory of Diffusion Processes and it is also used to represent the primitive of a white noise Gaussian process. To begin with though, we need the definition of the Itô stochastic integral.

Definition 2.2. An **Itô stochastic integral** (or just Itô integral) of f, denoted by $I[f]$, is given by

$$I[f] := \int_a^b f(t) dW(t) \tag{2.1}$$

where $W(t)$ is a Wiener process, $0 \leq a < b$ and f is a smooth non-anticipating function[1].

Now we can recall the definition of white noise process.

Definition 2.3. A **white noise Gaussian process**, $\xi := \xi(t)$, is the derivative in the sense of distributions of a Wiener process. Or

$$W(t) = \int_0^t \xi(t')dt'. \tag{2.2}$$

ξ has the following properties:

1. $\langle \xi(t) \rangle = 0$;
2. $\langle \xi(t)\xi(s) \rangle = \delta(t-s)$.

Here, we will call this process just white noise for simplicity.

We can now introduce the concept of stochastic differential equation.

Definition 2.4. A **Stochastic Differential Equation** (SDE) is a differential equation in which one or more terms are stochastic processes. The solution of such an equation is also a stochastic process.

We can think about the existence and uniqueness of the solutions of a SDE and, as well as in the ordinary differential equations, there exists a solution and it is unique (Theorem of Existence and Uniqueness for stochastic differential equations)[7].

Since, by 2. and 3. from Definition 2.1, the increments of W are independent with mean zero and of same law for u constant, the random variables $\xi(t)$ are, formally, independent and with same zero mean law.

For the modelization, it is often useful to think about a *stochastic differential equation* where $\xi(t)$ represents some fluctuations, for instance, let us suppose the following equation:

$$\frac{dx(t)}{dt} = \alpha x(t) + x(t)\xi(t), \text{ for a constant } \alpha > 0. \tag{2.3}$$

The trajectories $t \to W_t$ although continuous, are not differentiable $\forall t > 0$ so that the formal notation $\frac{dW}{dt} = \xi(t)$ must be carefully reinterpreted (see section A of Appendix). To stress this, the above stochastic differential equation is written

$$dx(t) = \alpha x(t)dt + x(t)dW(t). \tag{2.4}$$

The associated calculus is due to Kiyosi Itô.

An example: the Ornstein–Uhlenbeck process

The Ornstein–Uhlenbeck process, $x(t)$, is such that

$$dx(t) = \theta\left(\nu - x(t)\right)dt - \sigma dW(t) \tag{2.5}$$

[1] A function $f := f(t)$, where $f : [0, +\infty[\to \mathbb{R}$, is a *non-anticipating function of t* (also known as an *adapted process*) if $\forall s,t$ such that $t < s$, $f(t)$ is statistically independent of $W(s) - W(t)$ where $W(t)$ is Wiener process [10]

where $\theta, \sigma > 0$ and ν are parameters and $W(t)$ is a Wiener process as defined before.

Such a process can describe the velocity of a Brownian particle in which there is a friction term acting which we will discuss in the next chapter.

2.2 Numerical implementation

To obtain a numerical solution of a SDE, in this work, we are going to use the Euler-Maruyama Method (EMM) following references [8] and [9]. This method is a generalization of the Euler Method for ordinary differential equations to stochastic differential equations. EMM is based on the definition of the Itô integral.

Suppose the following stochastic differential equation, where f and g are given functions:

$$\frac{dx(t)}{dt} = f(x(t)) + g(x(t))\,\xi(t) \tag{2.6}$$

which can be written as

$$dx(t) = f(x(t))\,dt + g(x(t))\,dW(t) \tag{2.7}$$

with initial condition $x(0) = x_0$, $t \in [0,T]$, $W(t)$ is a Wiener process and $\xi(t)$ is a white noise process.

Then, $x(t)$ is a solution of the previous SDE if $x(t)$ solves the integral equation

$$x(t) - x(0) = \int_0^t f(x(s))\,ds + \int_0^t g(x(s))\,dW(s). \tag{2.8}$$

In order to obtain a numerical approximation of the solution, first we discretize the interval $[0,T]$ in N subintervals: let $\Delta t = \frac{T}{N}$ and $t_n = n\Delta t$.

Note that the initial value x_0 is given.

The exact solution is

$$x(t_{n+1}) = x(t_n) + \int_{t_n}^{t_{n+1}} f(x(s))\,ds + \int_{t_n}^{t_{n+1}} g(x(s))\,dW(s) \tag{2.9}$$

and so now we can compute $x_n \approx x(t_n)$ using the EMM and then we obtain

$$x_{n+1} = x_n + \Delta t\, f(x_n) + \Delta W_n g(x_n), \tag{2.10}$$

where $\Delta W_n = W(t_{n+1}) - W(t_n)$[2].

Regarding the convergence, we want to see how $|x_N - x(t_N)| \to 0$ as $\Delta t \to 0$. In order to do this, we must study both the strong and weak convergence, which give us the rate at which the mean of the error decreases as the time step converges to zero and the rate at which the error of the mean decreases as the time step converges to zero, respectively.

A numerical approximation x_N of the process x, with Δt the time step considered as before, is said to be of strong order of convergence s to x if for any fixed time t_N it holds

$$\mathbb{E}\left[|x_N - x(t_N)|\right] \leq K_1 \Delta t^s, \forall \Delta t < \delta \tag{2.11}$$

[2]The implementation of ΔW_n in C++ is `sqrt(`Δt`)`$\times$`r`, where `r` is a random number.

where K_1 is a constant and $\delta > 0$.

We say that a numerical approximation x_N of the process x, with Δt the time step defined before, is weakly convergent of order w to x if for any fixed time t_N and for any $2(w+1)$ continuous differentiable function h of polynomial growth we have

$$|\mathbb{E}[h(x_N)] - \mathbb{E}[h(x(t_N))]| \leq K_2 \Delta t^w, \forall \Delta t < \delta \tag{2.12}$$

where K_2 is a constant and $\delta > 0$.

EMM is strongly convergent with order 0.5 and weakly convergent with order 1 [9].

Chapter 3

Passive Brownian Particles

In this chapter we discuss the case of passive Brownian particles whose motion can be described by a Wiener process. We start with the historical origin of Brownian motion and then we introduce the Langevin approach to this problem. After this, we do some deductions, including the Stokes-Einstein equation.

3.1 Introduction

In 1827, the botanist Robert Brown observed pollen grains suspended in water through a microscope and he noticed that these grains perform a very erratic motion. This kind of motion was observed before Brown, but only in organic molecules and it was thought that this motion only occurred because the studied matter was *alive*. This explanation did not make sense to Brown, since he also was finding the same type of motion for inorganic particles. It was only in 1905 that Albert Einstein explained what was causing this motion, later denominated Brownian motion.

Consider a micron-size particle in a fluid. The fluid consists of atoms and/or molecules (much smaller than the particle) moving erratically due to thermal agitation and colliding among themselves and with the particle. If the density of the particle matches the one of the fluid and particle-particle aggregation is negligible, the particles remain in suspension. The motion of the particle is called Brownian and we denote such particles as passive Brownian particles.

At this point we should remark that about a century ago, the fact that matter is discrete and cannot be infinitely continously divided was not commonly thought of as scientific fact. Albert Einstein and Marian Smoluchowski declared that the existence of solvent molecules could be proven by the motion of particles in a suspension. What they also observed was that the mean square displacement of a particle turned out to be proportional to the length of the observation. This proportionality constant is associated to the diffusion coefficient, which plays an important role in one of the chapters of this thesis.

Whilst the zig-zag track of one passive Brownian particle might seem non-deterministic, when we look at the combined behaviour of many passive Brownian particles their motions can be rather useful. Being able to model the displacements of passive Brownian particles by a random process is the core of a probabilistic approach. Probability Calculus and Stochastic Processes theory find their backbone in the works of Einstein and Smoluchowski and nowadays are some of the most well known branches in mathematics. Besides physics, a wide range of other scientific disciplines now employ stochastic models with great success including biology, engineering and social sciences.

Even though the atomic theory was generally acknowledged by scientists in the late nineteenth century, a handful of prominent physicists claimed that atoms and molecules were not physical entities, but

were instead purely mathematical concepts that could be used for calculating the results of chemical reactions. These physicists saw matter as something continuous rather than something formed by discrete particles. Proving that this was not the case and that matter was indeed discontinuous turned out to be one of the great challenges in early twentieth century Physics. Jean Perrin, in 1908, through experimental work verified Einstein's hypothesis, which earned Perrin the 1926 Nobel Prize in Physics for his work on "the discontinuous structure of matter" in which he affirmed the atomic structure of matter [3].

Due to the randomness of the motion, we can treat Brownian motion as a stochastic process and to develop a phenomenological equation to describe Brownian motion.

To clarify, a *phenomenological model* is a hypothesized relationship between different phenomena, in a way which is consistent with fundamental theory, but is not directly derived from theory. What these models do, is to purely describe the relationship between variables while abstaining from clarifying why the variables interact in their particular ways. They also assume the described relationship exists beyond measured values.

One phenomenological equation to describe Brownian motion is the Langevin equation.

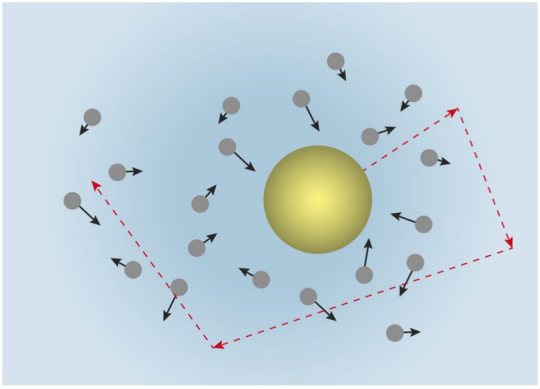

Figure 3.1: Brownian motion of the yellow particle, the passive Brownian particle. In red, we have the trajectory of the particle. The small grey particles represent the atoms or molecules of the suspending media. In black we have the direction of those grey particles. Source: Bembenek, Scott D., *Einstein's Paper on Brownian Motion.*, Scott D. Bembenek's Website: http://scottbembenek.com/einsteins-paper-on-brownian-motion/.

3.2 The Langevin approach

It is known that the random motion of passive Brownian particles is caused by a huge number of collisions with fluid molecules and so, instead of solving all of these equations of motion, we use a concept called the Langevin approach. In order to explain this approach, we will start with the following challenge:

Suppose that in a water droplet there are approximately 10^{20} *molecules of* H_2O *and a single passive Brownian particle (much larger than the* H_2O *molecules). Can you calculate the position of this passive Brownian particle at each instant?*

First, is it possible to do it **analytically**?

If we are supposing approximately 10^{20} particles then we would need approximately 10^{20} equations of motion, which is analytically impracticable.

So can we solve this problem **numerically**?

To answer to this question let us see if the best supercomputer in the world, *Sunway TaihuLight*, can

do it. This supercomputer has a memory of 1.3 PB[1], so the numerical implementation of 10^{20} equations of motion would imply to save in the memory, at least, 10^{20} values from the type `double` [2] which would cost approximately 10^{21} bytes, which is far larger than the available memory.

And so it can be concluded that it is not possible to solve this problem analytically neither numerically. Instead, we need to coarse-grain the effect of very frequent collisions with the fluid particles by the sum of a drag and a stochastic force. When we coarse-grain several degrees of freedom, we reduce a many-body problem into a **single-body** problem with a stochastic term.

3.2.1 Stochastic term

This stochastic term in our single-body problem describes the unbiased contribution of the interaction with the fluid at time t. We will assume white noise, $\vec{\xi}(t)$, to define the stochastic term, as defined in Definition 2.3 from the previous chapter. When attempting to model phenomena whereby the noise correlation time is far shorter than other time scales of interest, assuming white noise is advantageous. Suppose that this vector is a three dimensional vector which can be decomposed in x, y and z directions: $\vec{\xi}(t) = (\xi_x(t), \xi_y(t), \xi_z(t))$.

Recalling the Brownian motion definition from the previous chapter, we now have

$$W_k(t) := \int_0^t \xi_k\left(t'\right) dt', \text{ where } k \in \{x, y, z\}. \tag{3.1}$$

In this case the noise correlation time, affected by the (numerous) molecule impacts on the passive Brownian particle, is very small in comparison to the Brownian timescale, which corresponds to the time that it takes for the colloidal particle to explore a region of the order of its volume. This time is in the scale of $1s$. So, the timescale of interest (particle motion) is several orders of magnitude larger than the timescale of fluid/particle collision and uncorrelated collisions can be considered.

From the second law of Newton $\vec{F} = m\ddot{\vec{r}}(t)$, where $\vec{F}$ is the net force acting on the particle. For single isolated particles, we describe this force $\vec{F}$ as a sum of two contributions. The first is the frictional force (viscous drag) which represents the dynamical friction experienced by the particle, and we consider proportional to the velocity of the particle. This force is given by $-\gamma\dot{\vec{r}}(t)$. For small spheres and Stokes' regime, the friction coefficient, γ, is given by Stokes' law for spherical particles: $\gamma = 6\pi a\eta$. So, here we will suppose $\eta, a \neq 0$ and, thus $\gamma \neq 0$. The second contribution is regarded as a random and rapidly fluctuating force which we will consider to be described as white noise. We will represent this force by $\vec{\xi}(t)$. If we have no external forces, we can write

$$\vec{F} = -\gamma\dot{\vec{r}}(t) + \vec{\xi}(t),$$

and so

$$m\ddot{\vec{r}}(t) = -\gamma\dot{\vec{r}}(t) + \vec{\xi}(t), \tag{3.2}$$

which is known as the Langevin equation and it is an application of the SDE of which the solution is the Ornstein–Uhlenbeck process (see equation 2.5 from section 2.1 of the previous chapter) in physical sciences. We should refer that $\vec{r}(t)$ is a vector corresponding to three Wiener processes but we are using this notation since it is the Physics notation.

[1] PB means *petabytes*, *i.e.*, 10^{15} bytes

[2] Each `double` value needs 8 bytes in a computer.

We will consider two assumptions, $A1$ and $A2$.

$A1$) we assume that the mean of $\vec{\xi}$ is zero, *i.e.*

$$\left\langle \vec{\xi}(t) \right\rangle = \vec{0}$$

$A2$) the random force has a characteristic strength, Γ_T, which is uniform in time and space. The noise term is uncorrelated in time and space, *i.e.*,

$$\exists \Gamma_T \in \mathbb{R} \forall i,j \in \{x,y,z\} \forall t,t' \in \mathbb{R}_0^+ : \left\langle \xi_i(t)\xi_j(t') \right\rangle = \Gamma_T \delta_{ij} \delta(t-t'),$$

where δ represents the Dirac delta function and δ_{ij} the Kronecker delta.

3.2.2 Equations of motion

The motion of a passive Brownian particle is described by two coupled differential equations:

$$\begin{cases} \dot{\vec{r}} = \vec{v}(t) \\ m\dot{\vec{v}}(t) + \gamma\vec{v}(t) = \vec{\xi}(t) \end{cases} \tag{3.3}$$

The second equation of system 3.3 is an application of equation 2.5 from the previous chapter. We define Brownian dynamics as a simplified version of Langevin dynamics which corresponds to the limit where the inertia terms, $m\dot{\vec{v}}(t)$, are negligibly small. This approximation is typically known as *over-damped* Langevin dynamics or as Langevin dynamics *without inertia*. In Brownian dynamics, we neglect the term $m\dot{\vec{v}}(t)$ for times $t \gg {}^{m}/_{\gamma}$. So, if the iteration time scale Δt is larger than ${}^{m}/_{\gamma}$, overdamped Langevin dynamics is valid, because the relaxation of the suspending medium around the particle will occur in a time-scale that is shorter than the iteration time (*i.e.* below the numerical resolution).

3.3 Some important deductions

Here we are going to develop some important deductions that we will use later on.

3.3.1 First and second moments of the velocity

Defining $\vec{\xi}' := \frac{\vec{\xi}}{m}$ and $\tau := \frac{m}{\gamma}$, we can now replace it in equation 3.2 and so

$$\dot{\vec{v}}(t) + \frac{1}{\tau}\vec{v}(t) = \vec{\xi}'(t),$$

which $\forall k \in \{x,y,z\}$ as solution

$$v_k(t) = Ce^{-\frac{t}{\tau}} + e^{-\frac{t}{\tau}} \int_0^t e^{\frac{t'}{\tau}} \xi_k'(t')dt', \text{ where } C \text{ is a constant.}$$

Let us now calculate C

$$v_k(0) = Ce^0 + e^0 \int_0^0 e^{\frac{t'}{\tau}} \xi_k'(t')dt' = C \cdot 1 + 1 \cdot 0 = C$$

$$\therefore \vec{v}(t) = \vec{v}(0)e^{-\frac{t}{\tau}} + e^{-\frac{t}{\tau}} \int_0^t e^{\frac{t'}{\tau}} \vec{\xi}'(t')dt', \text{ which is the general solution.}$$

Averaging over an ensemble of particles we get

$$\begin{aligned} \langle v_k(t) \rangle &= \langle v_k(0) \rangle e^{-\frac{t}{\tau}} + e^{-\frac{t}{\tau}} \int_0^t e^{\frac{t'}{\tau}} \langle \xi_k'(t') \rangle dt' \\ \Leftrightarrow \langle v_k(t) \rangle &= \langle v_k(0) \rangle e^{-\frac{t}{\tau}}, \end{aligned}$$

and from this we conclude that

$$\langle \vec{v}(t) \rangle = (\langle v_x(0) \rangle, \langle v_y(0) \rangle, \langle v_z(0) \rangle) e^{-\frac{t}{\tau}},$$

so the average velocity decays exponentially in time and τ sets the timescale for relaxation.

Let us now calculate $\langle v_k^2(t) \rangle$ *i.e.* the ensemble average of $v_k^2(t)$.

Let $k, l \in \{x, y, z\}$ be two arbitrary directions and t, t' two arbitrary time instants. $v_k(0)$ and $v_l(0)$ are constants and from Assumption 1 (see section 3.2.1) we have

$$\langle v_k(t)v_l(t') \rangle = e^{-\frac{t+t'}{\tau}} \langle v_k(0)v_l(0) \rangle + e^{-\frac{t+t'}{\tau}} \int_0^t \int_0^{t'} e^{\frac{t_0+t_0'}{\tau}} \langle \xi_k'(t_0)\xi_l'(t_0') \rangle dt_0 dt_0'.$$

From Assumption 2 (see section 3.2.1), and supposing $k = l$

$$\begin{aligned} \langle v_k(t)v_k(t') \rangle &= e^{-\frac{t+t'}{\tau}} \langle v_k^2(0) \rangle + e^{-\frac{t+t'}{\tau}} \frac{\Gamma_T}{m^2} \int_0^{t'} \int_0^t e^{\frac{t_0+t_0'}{\tau}} \delta(t_0 - t_0')dt_0 dt_0' \\ &= e^{-\frac{t+t'}{\tau}} \langle v_k^2(0) \rangle + e^{-\frac{t+t'}{\tau}} \frac{\Gamma_T}{m^2} \int_0^{t'} e^{\frac{2t_0'}{\tau}} dt_0' \\ &= e^{-\frac{t+t'}{\tau}} \langle v_k^2(0) \rangle + e^{-\frac{t+t'}{\tau}} \frac{\Gamma_T \tau}{2m^2} \left(e^{\frac{2t'}{\tau}} - 1 \right). \end{aligned}$$

Let $t = t'$, and then

$$\langle v_k^2(t) \rangle = e^{\frac{-2t}{\tau}} \langle v_k^2(0) \rangle + \frac{\Gamma_T \tau}{2m^2} \left(1 - e^{\frac{-2t}{\tau}} \right).$$

We know that

$$\langle \vec{v}^2(t) \rangle = \langle v_x^2(t) \rangle + \langle v_y^2(t) \rangle + \langle v_z^2(t) \rangle,$$

then

$$\langle \vec{v}^2(t) \rangle = e^{\frac{-2t}{\tau}} \langle \vec{v}^2(0) \rangle + \frac{d\Gamma_T \tau}{2m^2} \left(1 - e^{\frac{-2t}{\tau}} \right). \tag{3.4}$$

By the Equipartition Theorem [12], we know that, at equilibrium, each degree of freedom contributes with $\frac{1}{2}k_BT$ to the average energy per particle, so:

$$\frac{1}{2}m \langle \vec{v}^2(t) \rangle = \frac{dk_BT}{2} \Rightarrow \frac{1}{2}md \langle v_k^2(t) \rangle = \frac{dk_BT}{2} \text{ where } d = 1, 2, 3.$$

Taking the limit $t \to \infty$ (here the system necessarily reaches equilibrium) in equation 3.4 we conclude that

$$m\frac{\Gamma_T \tau}{2m^2} = k_BT \Rightarrow \Gamma_T = \frac{2mk_BT}{\tau} = 2\gamma k_BT$$

and then, from Assumption 2 (see section 3.2.1) we have

$$\forall i,j \in \{x,y,z\} \forall t,t' \in \mathbb{R}_0^+ : \left\langle \xi_i(t)\xi_j(t') \right\rangle = 2\gamma k_B T \delta_{ij} \delta(t-t'). \tag{3.5}$$

3.3.2 The Stokes-Einstein equation

In order to obtain $\vec{r}(t)$ we should integrate $\vec{v}(t)$, which will be designated here by $\vec{R}(t)$ instead of $\vec{r}(t)$ to avoid confusion with $\vec{r}(t)$ for the Brownian dynamics. We supposed $R_i(0) = 0$.

So,

$$\int_0^t \vec{v}(t'')dt'' = \int_0^t e^{-\frac{t''}{\tau}} \left(\vec{v}(0) + \int_0^{t''} e^{\frac{t'}{\tau}} \vec{\xi}'(t')dt' \right) dt''.$$

Then, $\forall i \in \{x,y,z\}$ and for some $t \geqslant 0$ we have

$$\begin{aligned}
R_i(t) &= \int_0^t \left(e^{-\frac{t''}{\tau}} v_i(0) + e^{-\frac{t''}{\tau}} \int_0^{t''} e^{\frac{t'}{\tau}} \xi_i'(t')dt' \right) dt'' \\
&= -\tau v_i(0) \left(e^{-\frac{t}{\tau}} - 1 \right) + \int_0^t \int_{t'}^t e^{-\frac{t''}{\tau}} e^{\frac{t'}{\tau}} \xi_i'(t')dt''dt', \text{ by Fubini's Theorem} \\
&= -\tau v_i(0) \left(e^{-\frac{t}{\tau}} - 1 \right) - \tau \int_0^t \left(e^{\frac{t'-t}{\tau}} - 1 \right) \xi_i'(t')dt'.
\end{aligned}$$

Now, let us suppose two arbitrary directions $i,j \in \{x,y,z\}$. Then

$$\begin{aligned}
\left\langle R_i(t)R_j(t) \right\rangle &= \tau^2 \left\langle v_i(0)v_j(0) \right\rangle \left(e^{-\frac{t}{\tau}} - 1 \right)^2 + \\
&+ \tau^2 \int_0^t \int_0^t \left(e^{\frac{t'-t}{\tau}} - 1 \right) \left(e^{\frac{t''-t}{\tau}} - 1 \right) \frac{2\gamma k_B T}{m^2} \delta_{ij} \delta(t'-t'')dt'dt'' \\
&= \tau^2 \left\langle v_i(0)v_j(0) \right\rangle \left(e^{-\frac{t}{\tau}} - 1 \right)^2 + 2\frac{m^2}{\gamma^2} \frac{\gamma k_B T}{m^2} \delta_{ij} \int_0^t \left(e^{\frac{t''-t}{\tau}} - 1 \right)^2 dt'' \\
&= \tau^2 \left\langle v_i(0)v_j(0) \right\rangle \left(e^{-\frac{t}{\tau}} - 1 \right)^2 + 2\frac{k_B T}{\gamma} \delta_{ij} \int_0^t \left(e^{\frac{2t''-2t}{\tau}} - 2e^{\frac{t''-t}{\tau}} + 1 \right) dt'' \\
&= \tau^2 \left\langle v_i(0)v_j(0) \right\rangle \left(e^{-\frac{t}{\tau}} - 1 \right)^2 + 2\frac{k_B T}{\gamma} \delta_{ij} \left[\frac{\tau}{2} \left(1 - e^{\frac{-2t}{\tau}} \right) - 2\tau \left(1 - e^{-\frac{t}{\tau}} \right) + t \right]
\end{aligned}$$

and now supposing $i = j$ we obtain

$$\left\langle R_i^2(t) \right\rangle = \tau^2 \left\langle v_i^2(0) \right\rangle \left(e^{-\frac{t}{\tau}} - 1 \right)^2 + 2\frac{k_B T}{\gamma} \left[\frac{\tau}{2} \left(1 - e^{\frac{-2t}{\tau}} \right) - 2\tau \left(1 - e^{-\frac{t}{\tau}} \right) + t \right].$$

When $t \gg 1$:

$$\left\langle R_k^2(t) \right\rangle \sim 2\frac{k_B T}{\gamma} t \Rightarrow \left\langle \vec{R}^2(t) \right\rangle \sim 2d\frac{k_B T}{\gamma} t.$$

From Brownian dynamics (section 3.3.3) we have $\left\langle \vec{r}^2(t) \right\rangle \sim 2D_T dt$ and so,

$$\left\langle \vec{r}^2(t) \right\rangle = \lim_{t \gg 1} \left\langle \vec{R}^2(t) \right\rangle \Leftrightarrow 2dD_T t = 2d\frac{k_B T}{\gamma} t$$

from which we conclude that

$$D_T = \frac{k_B T}{\gamma},$$

which is the well-known Stokes–Einstein equation.

3.3.3 Mean square displacement

$\forall k \in \{x,y,z\}$ we have

$$\frac{dr_k}{dt} = \frac{\xi_k(t)}{\gamma} \Rightarrow \int_{r_k(0)}^{r_k(t)} dr_k = \int_0^t \frac{\xi_k(t')}{\gamma} dt',$$

then

$$r_k(t) - r_k(0) = \int_0^t \frac{\xi_k(t')}{\gamma} dt'$$

and if $r_k(0) = 0$, we have

$$r_k(t) = \int_0^t \frac{\xi_k(t')}{\gamma} dt'.$$

Now, let us take the ensemble average of $r_k(t)$

$$\langle r_k(t) \rangle = \left\langle \int_0^t \frac{\xi_k(t')}{\gamma} dt' \right\rangle = \int_0^t \frac{\langle \xi_k(t') \rangle}{\gamma} dt' = 0.$$

For the ensemble average of $r_k^2(t)$,

$$\begin{aligned}
\left\langle r^2{}_k(t) \right\rangle &= \left\langle \int_0^t \frac{\xi_k(t')}{\gamma} dt' \int_0^t \frac{\xi_k(t'')}{\gamma} dt'' \right\rangle \\
&= \int_0^t \int_0^t \frac{\langle \xi_k(t')\xi_k(t'') \rangle}{\gamma^2} dt' dt'' \\
&= \int_0^t \int_0^t \frac{2\gamma k_B T \delta(t'-t'')}{\gamma^2} dt' dt'' \\
&= 2D_T \int_0^t dt'' \\
&= 2D_T t.
\end{aligned}$$

Then

$$\left\langle \vec{r}^2(t) \right\rangle = \left\langle r^2{}_x(t) \right\rangle + \left\langle r^2{}_y(t) \right\rangle + \left\langle r^2{}_z(t) \right\rangle = 2dD_T t \tag{3.6}$$

$$\therefore \begin{cases} \langle \vec{r}(t) \rangle = \vec{0} \\ \left\langle \vec{r}^2(t) \right\rangle = 2dD_T t \end{cases}.$$

Since $\langle \vec{r}(t) \rangle = \vec{0}$, we conclude that there is a spatial homogeneity, *i.e.* there is no preferential direction of the motion. From $\left\langle \vec{r}^2(t) \right\rangle = 2dD_T t$ we conclude that the mean square displacement, $\left\langle \vec{r}^2(t) \right\rangle$, is linear in time.

In Itô's Stochastic Calculus, the equation $(dW(t))^2 = dt$ means $\left\langle \vec{r}^2(t) \right\rangle = 2dD_T t$ [15].

Chapter 4

Active particles

In this chapter we introduce the concept of active particles, their relevance and how they differ from their passive counterpart (passive Brownian particles).

4.1 What are active particles?

Active motion is a phenomenon which we can observe across a broad spectrum of systems. We call active particles the particles which show an active motion. We can find synthetic active particles, such as those micro-jets in Figure 4.1, and active particles created by Nature, as e.g. the spermatozoa in Figure 4.2. In Nature, one can find numerous biological examples across different size scales, varying from active motion in cells and micro-organisms, up to higher organisms such as flocks of birds and schools of fish. Another example is the collective motion of vehicles and pedestrians. For self-propelled active motion to happen there is the necessity of energy consumption and it may involve processes of energy storage.

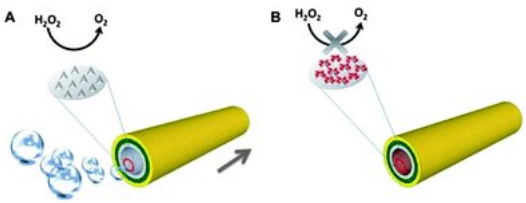

Figure 4.1: An example of active particles is a catalytic micro-jet. Micro-jets are made using rolled-up nanotechnology. Micro-jets are created by rolling up sheets of nano-material. In the past few years, these micro-jets have shown great potential for many applications within the field of nanorobotics. In the future these catalytic micro-jet particles may be used in active bio-sensing systems. What is lacking though, is a theoretical model accurate enough to describe the self propulsion mechanism as well as the origin of motion [4].

The word **active** implies that a Brownian particle can remove energy from the medium, store it in an internal depot, and then convert this internal energy into kinetic energy.

Both passive Brownian and active particles have their motion driven by equilibrium thermal fluctuations caused by random collisions with the molecules of the medium they are in. The difference is that active particles are also able to propel themselves. This active swimming coupled with the random collisions takes them far from an equilibrium state. To find statistical models that describe this phenomenon is a challenge to theoretical physicists these days.

As an example of where such phenomena are encountered, we can highlight some applications: bacterial processes such as gene expression, motility and biological pattern formation (e.g. biofilm for-

Figure 4.2: Spermatozoa motion is a good example of active motion. Source: AMP - Lab GmbH, CASAnova

mation) [2]. Another good example is found in directed transport and molecular motors where the ability of living cells to generate motion and forces can be described by active motion.

Inspired by these motile microorganisms, researchers have been trying to develop artificial active particles; these manmade micro- and nano-machines could lead us to autonomous agents for healthcare, sustainability, and security applications [1].

4.2 Equations of motion

Let $\vec{F^T} := \vec{F^T}(t)$ be a thrust term. The particle tends to move on the same direction of each movement, so we will define this term as $\vec{F^T}(t) = \alpha \cdot v_{\text{drift}} \vec{u}(t)$, where $v_{\text{drift}} \neq 0$ represents the absolute value of thrust velocity or drift velocity. We define α as a real parameter such that $[\alpha] = \left[\frac{M}{T}\right]$.

4.2.1 Two-dimensional case

Here, we will study the two-dimensional case, *i.e.* $d = 2$, and so we will define $\vec{u}(t)$ as a unitary vector with thrust direction given by

$$\vec{u}(t) := (cos(\varphi(t)), sin(\varphi(t))), \tag{4.1}$$

where $\varphi(t)$ represents the angle between the x-axis and the thrust direction at instant t, $\vec{u}(t)$.

In the two-dimensional case the equations of motion of an active particle are three coupled differential equations,

$$\begin{cases} \dot{\vec{r}} = \vec{v}(t) \\ m\dot{\vec{v}}(t) = -\gamma\vec{v}(t) + \vec{\xi}(t) + \vec{F^T}(t) \\ \dot{\varphi}(t) = \xi_\varphi(t) \end{cases} \tag{4.2}$$

where $\xi_\varphi(t)$ is a function that we will define in the next chapter.

The second equation from system 4.2 is an application of a SDE similar to equation 2.5 but now with time-dependent coefficients [5].

4.2.2 Short note about one and three-dimensional cases

Here, we are interested in the two-dimensional case and so we will not focus on one and three-dimensional cases.

For the one-dimensional case we can think in two different ways:

- We can define a unitary vector with the direction of the motion.

• Or we can think in a *quasi*-1D situation in which we define the vector as $\vec{u}(t) := cos\,(\varphi(t))$, relating it with the two-dimensional case. Here, $cos\,(\varphi(t))$ is the same which was defined in equation 4.1.

For the three-dimensional case, the equations of motion depend on translational and rotational degrees of freedom.

Chapter 5

General Framework

5.1 Theory

Hereafter, we will consider a two-dimensional system.

From the previous chapter, we can write the general equations which describe the motion of active or passive particles, since when the thrust term defined in Section 4.2 is null, *i.e.* $\vec{F^T}(t) = \vec{0}$, we have the equations for the motion of a passive particle, *i.e.*, the motion of a passive particle is a particular case of the motion of an active particle.

5.1.1 General equations of Langevin overdamped Dynamics

In Langevin overdamped Dynamics we consider $m\dot{\vec{v}}(t) \approx 0$, so

$$\begin{cases} \dot{\vec{r}}(t) = \vec{v}(t) \\ 0 = -\gamma\vec{v}(t) + \vec{\xi}(t) + \vec{F^T}(t) \ , \\ \dot{\varphi}(t) = \xi_\varphi(t) \end{cases} \tag{5.1}$$

where $\vec{u}(t) := (cos\varphi(t), sin\varphi(t))$, and $\varphi(t)$ is the angle between the x-axis and the thrust direction at instant t, $\vec{u}(t)$.

We will write $\vec{\xi}$ as a vector of two components representing two spatial dimensions: $\vec{\xi} := (\xi_x, \xi_y)$.

Let w_φ, w_x and w_y represent independent white Gaussian noise stochastic processes with zero mean and unitary variance.

Denote $\vec{w}$ by $\vec{w} := (w_x, w_y)$.

We define ξ_φ, ξ_x and ξ_y such that:

$$\begin{cases} \xi_\varphi(t) = A_\varphi \cdot w_\varphi(t) \\ \xi_x(t) = A_x \cdot w_x(t) \\ \xi_y(t) = A_y \cdot w_y(t) \end{cases} \tag{5.2}$$

where A_i is the amplitude of the noise ξ_i, $i \in \{x, y, \varphi\}$.

Our goal now is to find the values for A_i.

Firstly, since there is no preferential direction, let us set $A_x = A_y =: A$.

We know that ξ_x and ξ_y have amplitude given by the square root of $\Gamma_T = 2\gamma^2 D_T$ (from equation 3.5 of Chapter 3).

So, let us now find the amplitude of ξ_φ, which is given by the square root of a constant, Γ_R.

Let us say that this is for one particle.

Suppose that ξ_φ has the following property: $\langle \xi_\varphi(t)\xi_\varphi(t')\rangle = \Gamma_R\delta(t-t')$, where δ is the Dirac Delta function and Γ_R is some factor that we must find in the next steps. This noise will generate changes in the rotational degree of freedom, so we want to relate it with φ.

We know that for the rotational diffusion, the mean square angular deviation with respect to time is asymptotically Brownian, *i.e.*

$$\langle \varphi^2(t)\rangle \sim 2D_R t. \tag{5.3}$$

From equations 5.1 we know that

$$\dot{\varphi}(t) = \xi_\varphi(t)$$

then we can write

$$\varphi(t) = \int_0^t \xi_\varphi(t')dt'.$$

So, let t and t' be two arbitrary instants,

$$\begin{aligned}\langle \varphi(t)\varphi(t')\rangle &= \left\langle \int_0^t \int_0^{t'} \xi_\varphi(t_1)\xi_\varphi(t_2)dt_1dt_2 \right\rangle \\ &= \int_0^t \int_0^{t'} \Gamma_R\delta(t_1-t_2)dt_1dt_2 \\ &= \Gamma_R t,\end{aligned}$$

then we conclude that

$$\langle \varphi^2(t)\rangle = \Gamma_R t.$$

From equation 5.3 and the last equation:

$$\Gamma_R t = 2D_R t \Rightarrow \Gamma_R = 2D_R.$$

Then, $A_\varphi = \sqrt{2D_R}$.

Another way of defining the noise is by the process of each of its components.

Supposing N particles then we have $3N$ degrees of freedom, *i.e.* for each particle we have two degrees of freedom for the translation motion and one for the rotational motion.

5.2 Numerical implementation

Theoretically, we know that:

$$\begin{cases} \xi_i(t) = A\cdot w_i(t), i \in \{x,y\} \\ \xi_\varphi(t) = A_\varphi \cdot w_\varphi(t) \end{cases}$$

where

- $A = \sqrt{\Gamma_T}$;
- $\Gamma_T = 2\gamma^2 D_T$;
- $A_\varphi = \sqrt{\Gamma_R}$;
- $\Gamma_R = 2D_R$.

In order to obtain $\vec{r}$ numerically we need to discretize time.

Question: how should the random numbers (which will be used in the simulations) be defined?

We know that $\forall i,j \in \{x,y\} \forall t,t' \geqslant 0 : \left\langle \xi_i(t)\xi_j(t') \right\rangle = \Gamma_T \delta_{ij} \delta(t-t')$, in the continuous domain, *i.e.*, in $[0,t_f]$ where t_f is some fixed positive real value representing the final instant of some simulation.

Now, let us discretize the domain:

- we discretize the interval $[0,t_f]$ in time steps of size Δt, such that we have $\frac{t_f}{\Delta t}$ time steps.
- In each time step Δt, we consider that the position of the particle is displaced by ζ_j such that

For passive particles, $\forall i \in \{x,y\}$ and $t \geqslant 0$:

$$r_i(t) = \sum_{k=1}^{\frac{t}{\Delta t}} \zeta_k, \text{ with } \zeta_k = \int_{(k-1)\Delta t}^{k\Delta_t} \xi_i(t')dt'.$$

Hence, $\forall k = 1,...,\frac{t}{\Delta t} : \langle \zeta_k \rangle = 0$ trivially, and $\forall k,l = 1,...,\frac{t}{\Delta t}$ and $\forall i,j \in \{x,y\}$

$$\begin{aligned}
\langle \zeta_k \zeta_l \rangle &= \int_{(k-1)\Delta t}^{k\Delta t} \int_{(l-1)\Delta t}^{l\Delta t} \left\langle \xi_i(t_1)\xi_j(t_2) \right\rangle dt_1 dt_2 \\
&= \int_{(k-1)\Delta t}^{k\Delta t} 2\gamma^2 D_T dt_2 \\
&= 2\gamma^2 D_T \Delta t.
\end{aligned}$$

Note that, it is now straightforward to check that $\vec{\xi}$ has units of force. Dirac delta function has the same units as the units of the inverse of its argument, *i.e.* $[\delta(t)] = \frac{1}{[T]}$ And so

$$[\xi_i] = \left[\sqrt{2\gamma^2 D_T \Delta t}\right] \frac{1}{[T]} = \left[\frac{M^2}{T^2} \cdot \frac{L^2}{T} \cdot T\right]^{\frac{1}{2}} \frac{1}{[T]} = \left[\frac{M \cdot L}{T^2}\right].$$

Now, we will see the influence of rotation in numerically terms.

We know that $\forall t,t' \geqslant 0 : \left\langle \xi_\varphi(t)\xi_\varphi(t') \right\rangle = \Gamma_R \delta(t-t')$, in the continuous domain, *i.e.* in $[0,t_f]$ where t_f is some fixed positive real value representing the final instant of some simulation.

Now, let us discretize the domain:

- in each time step Δt we consider rotational displacements ψ_j,$\forall t \geqslant 0$, such that

$$\varphi(t) = \sum_{j=1}^{\frac{t}{\Delta t}} \psi_j, \text{ with } \psi_j = \int_{(j-1)\Delta_t}^{j\Delta t} \xi_\varphi(t')dt'.$$

Hence, $\forall k = 1,...,\frac{t}{\Delta t} : \langle \psi_k \rangle = 0$ trivially, and $\forall k,l = 1,...,\frac{t}{\Delta t}$

$$\begin{aligned}\langle \psi_k \psi_l \rangle &= \int_{(k-1)\Delta t}^{k\Delta t} \int_{(l-1)\Delta t}^{l\Delta t} \left\langle \xi_\varphi(t_1)\xi_\varphi(t_2) \right\rangle dt_1 dt_2 \\ &= \int_{(k-1)\Delta t}^{k\Delta t} 2D_R dt_2 \\ &= 2D_R\Delta t.\end{aligned}$$

Then, **numerically**, we have:

• for the translation motion we need a random number generator with Gaussian distribution, zero mean and variance = $2\gamma^2 D_T \Delta t$ per degree of freedom in the translation motion. To do this, we can implement a random number generator per translational degree of freedom (which are the theoretical w_x and w_y of system 5.2) with Gaussian distribution, zero mean and unitary variance and then we multiply the obtained numbers by $\sqrt{2\gamma^2 D_T \Delta t}$.

• For the rotational motion we need a random number generator with Gaussian distribution, zero mean and variance = $2D_R\Delta t$. To do this, we can implement a generator (which is the theoretical w_φ of system 5.2) with Gaussian distribution, zero mean and unitary variance and then we multiply the obtained numbers by $\sqrt{2D_R\Delta t}$.

Random number generators: a short note

Numerically, we implemented three random number generators (two for translational motion and one for rotational motion), each given by a Gaussian distribution with zero mean, unitary variance and then we generated one million of random numbers with each generator [13].

These numbers were generated between -3 and 3 so that the probability of our variable x was $p(\mu - 3\sigma \leq x \leq \mu + 3\sigma) = 0.9973$, where $\mu = 0$ and $\sigma = 1$.

In order to check if these one million random numbers generated followed a Gaussian distribution with zero mean and unitary variance, we calculated their histograms and the respective mean and variance.

The results are in Figure 5.1, where the red curve is the probability density function given by $p(x) = \frac{exp\left(-\frac{1}{2}x^2\right)}{\sqrt{(2\pi)}}$ where x is a random number.

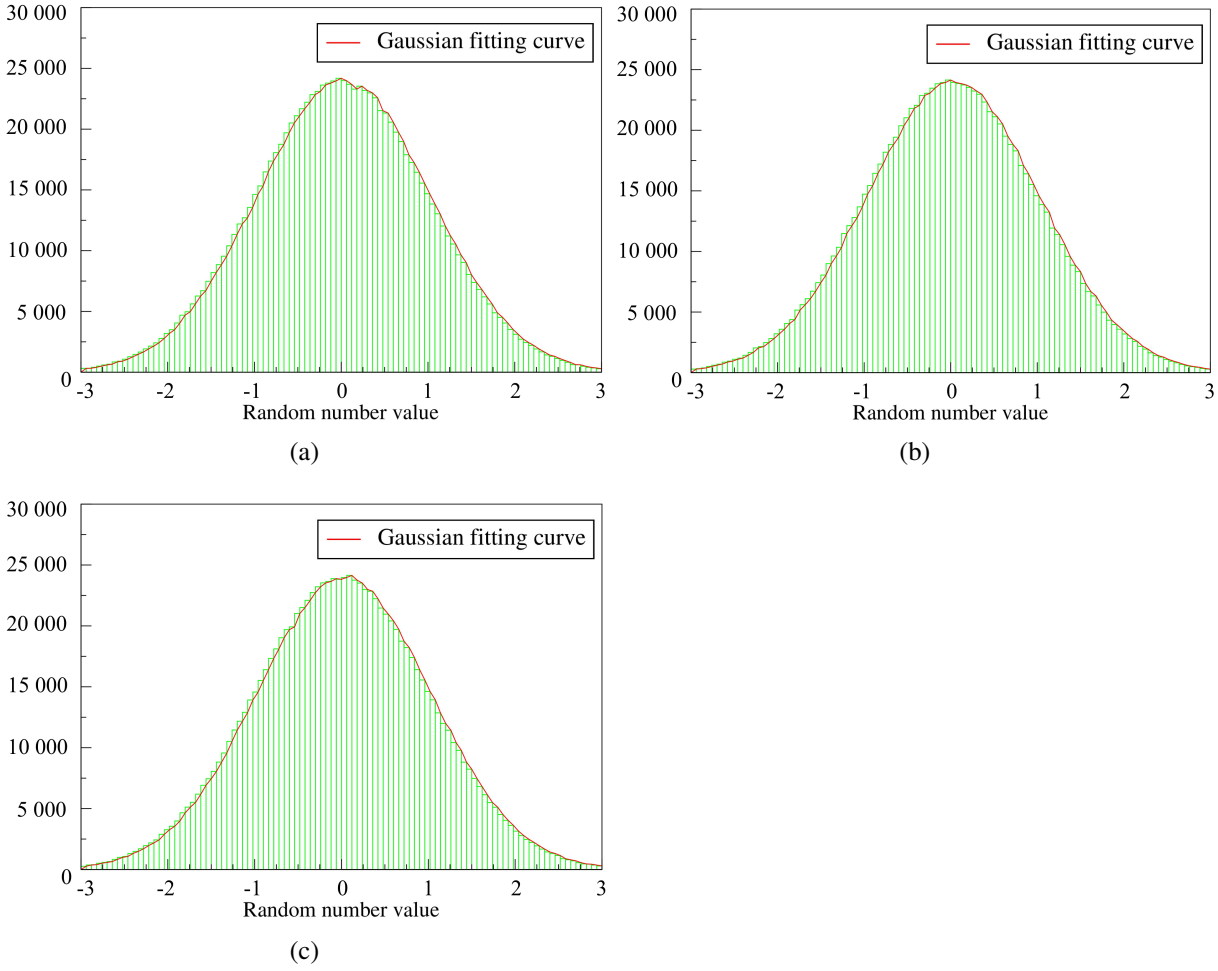

Figure 5.1: Histograms with data from the three random number generators. In (a), (b) and (c) it is represented the histogram correspondent to the random generator number which is theoretically represented by, respectively, w_x, w_y and w_φ from system 5.2.

The three histograms represented in Figure 5.1 have 10^2 bins of 10^6 random numbers obtained with different generators.

In Figure 5.1a these random numbers were obtained by a generator which is the theoretical w_x from system 5.2. The calculated mean was ≈ 0.0004 and the variance was ≈ 0.97. The random numbers used to plot the histogram of Figure 5.1b were obtained using a generator which is the theoretical w_y from system 5.2. For this generator the calculated mean was ≈ 0.0003 and the variance was ≈ 0.97. Finally, in Figure 5.1c a histogram is shown whereby the random numbers were obtained by a generator which is the theoretical w_φ from system 5.2. For this generator the calculated mean was ≈ -0.0003 and the variance was ≈ 0.98.

We should also include a remark about the initial angle: in order to have a good distribution for the initial angle of the particles in our simulations, we implemented a random number generator with uniform distribution between 0 and 2π.

5.2.1 Examples

It is to be remarked that in this work we will not include units of measurement when we refer to any value, parameter or variable. We assume that all of these values are in units of simulation as mentioned in section B of Appendix.

In order to observe an initial difference between the motion of passive Brownian and active particles, we performed simulations in which we implemented a concept called periodic boundary conditions (PBC).

The concept of PBC consists on using a small part of the actual system to approximate an (infinitley) larger system. This smaller part is called the unit cell and the PBC assume that a particle passing through the side of a unit cell, will emerge with equal velocity on the opposite side. In the two-dimensional case, the topological space created by the PBC can be thought of as being mapped onto a torus. Figure 5.2 represents an example of the implementation of PBC in two dimensions where we can observe particles (in red) and their direction of velocity (represented by the black arrows). The unit cell is represented in blue and surrounding it there are eight copies of this unit cell to give us a clear picture of what happens to the particles in the next iteration.

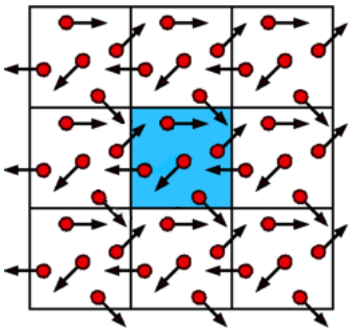

Figure 5.2: Example of the implementation of PBC in a two-dimensional system. Source: Adapted from *http://www.compsoc.man.ac.uk/ lucky/Democritus/Theory/pbc-mi.html*

To perform our simulations, we considered $L = 50$ and different values for v_{drift}, with $v_{drift} = 0$ representing passive Brownian particles and $v_{drift} > 0$ active particles. We started with the case whereby there were two particles in the system in order to study the difference of the trajectories between passive Brownian and active particles. Then we increased the number of particles in our system to 10^3 to study the behaviour of the mean square displacement, $\langle \vec{r}^2(t) \rangle$, when considering passive Brownian or active particles.

For our initial simulation conditions, we considered $\Delta t = 2 \times 10^{-3}$, 10^4 time steps and a system with two particles with the same initial position (the origin). In the first case we considered two passive Brownian particles, *i.e.* $v_{drift} = 0$, represented in Figure 5.3a, and in the second case we considered two active particles with a drift velocity value of $v_{drift} = 1$, represented in Figure 5.3b. In Figure 5.3b, the active particle with a blue trajectory was considered to have an initial thrust direction angle of $\varphi(0) = 0$ radians while the particle with the orange trajectory was considered to have an initial thrust direction of $\varphi(0) = \pi$ radians. Figures 5.3a and 5.3b clearly display a difference in motion of the particles. In Figure 5.3a we see a totally random motion of two particles while in Figure 5.3b we see a type of motion with a direction although we can observe some directional fluctuations. We can also observe that for the active case the particles move over longer distances, for the same time interval.

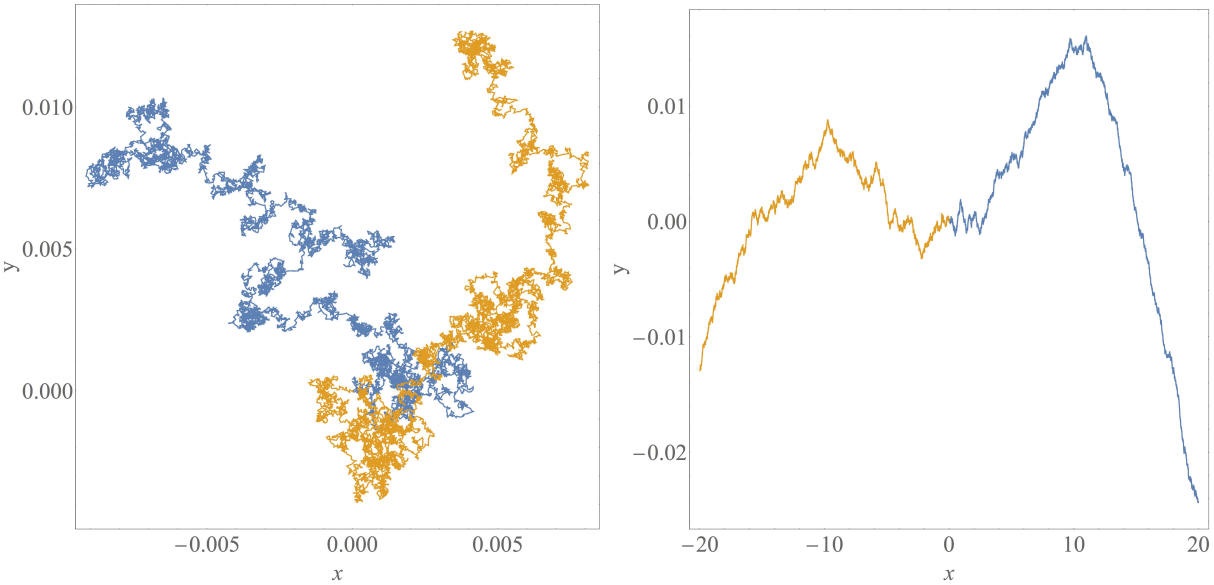

(a) $v_{drift} = 0$ (b) $v_{drift} = 1$

Figure 5.3: Trajectories of two particles, one in orange and another in blue, when considering: two passive Brownian particles, *i.e.* $v_{drift} = 0$, in (a), and two active particles with a drift velocity value of $v_{drift} = 1$, in (b).

Our next step was to study the mean square displacement, $\langle \vec{r}^2(t) \rangle$, for passive Brownian and active particles. In order to do this we considered 10^3 particles in our simulations and here we fixed $\Delta t = 2 \times 10^{-2}$. We considered $D_R = 0.15$. We divided this study into two cases: one in which the total simulation time is smaller than the inverse of the rotational coefficient, represented in Figures 5.4 and 5.5, and another whereby the total simulation time is much larger, represented in Figures 5.6 and 5.7. In our studies, we plotted the linear scale of $\langle \vec{r}^2(t) \rangle$ *vs* t and then the logarithmic scale of this relation to better understand the difference of the behaviour of $\langle \vec{r}^2(t) \rangle$ over time. In each of the following four figures, Figures 5.4-5.7, we depict two plots: the red and blue plots are, respectively, the linear and the logarithmic scale of $\langle \vec{r}^2(t) \rangle$ *vs* t.

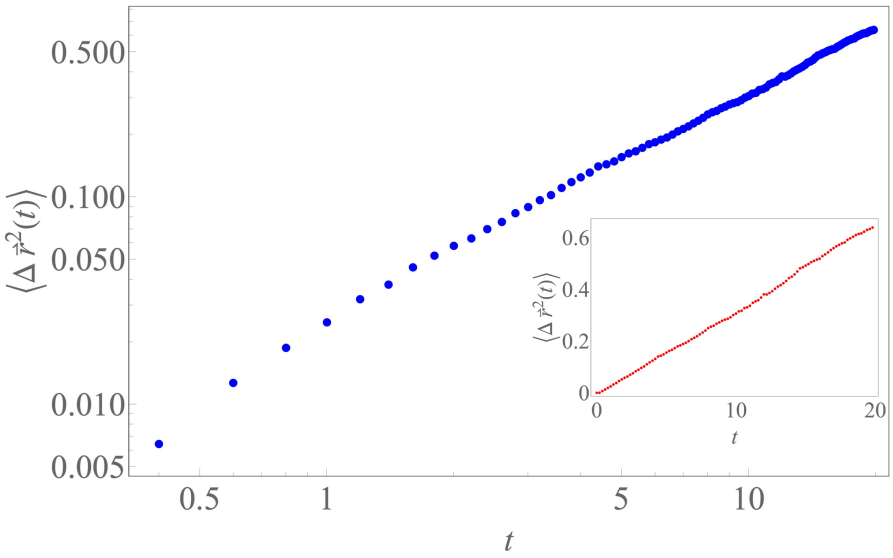

Figure 5.4: Mean square displacement for simulations performed considering passive Brownian particles, $\Delta t = 2 \times 10^{-2}$ and 20 as the total simulation time. The logarithmic scale is represented in blue and the linear scale in red.

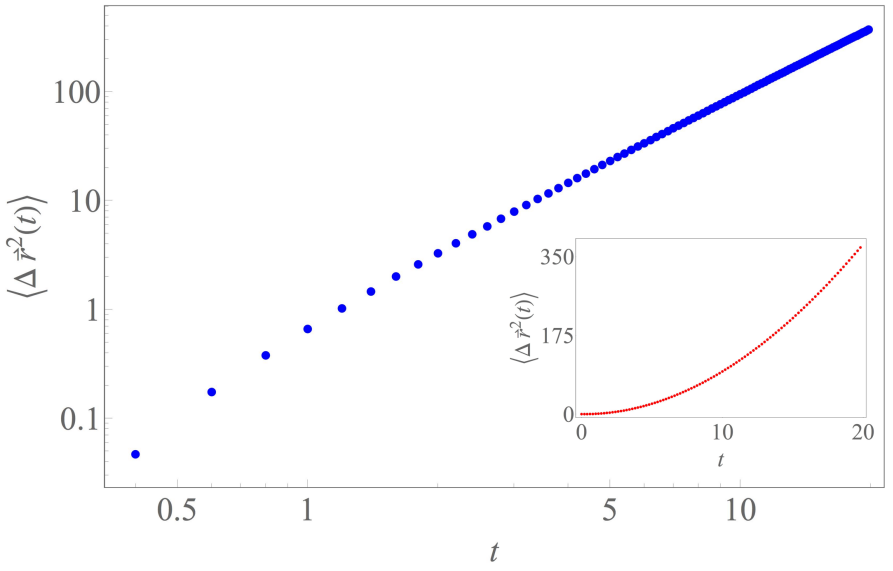

Figure 5.5: Mean square displacement for simulations performed considering active particles with $v_{drift} = 1$, $\Delta t = 2 \times 10^{-2}$ and 20 as the total simulation time. The logarithmic scale is represented in blue and the linear scale in red.

By observing the passive Brownian case in Figure 5.4, we can see that for passive Brownian particles there is a linear dependence of $\langle \vec{r}^2(t) \rangle$ with the time while, when observing the active case in Figure 5.5,

we see that for active particles (here considered with drift velocity of $v_{drift} = 1$) there is a quadratic dependence between them since the calculated the slopes of the lines in $log\left(\left\langle \vec{r}^2(t)\right\rangle\right)$ *vs* $log(t)$ were 1.00 ± 0.04 for the slope related to the case in Figure 5.4 and 2.03 ± 0.05 for the slope related to the case in Figure 5.5. So for passive Brownian particles there is a diffusive behaviour and for active particles (here considered with $v_{drift} = 1$) the behaviour is ballistic.

But what happens if we increase the total simulation time? For this case we considered 20 000 as the total simulation time which is much lager than the 20 total simulation time as in the previous case. In order to study the impact of a longer total simulation time, we performed simulations considering again $\Delta t = 2 \times 10^{-2}$ and 10^3 particles.

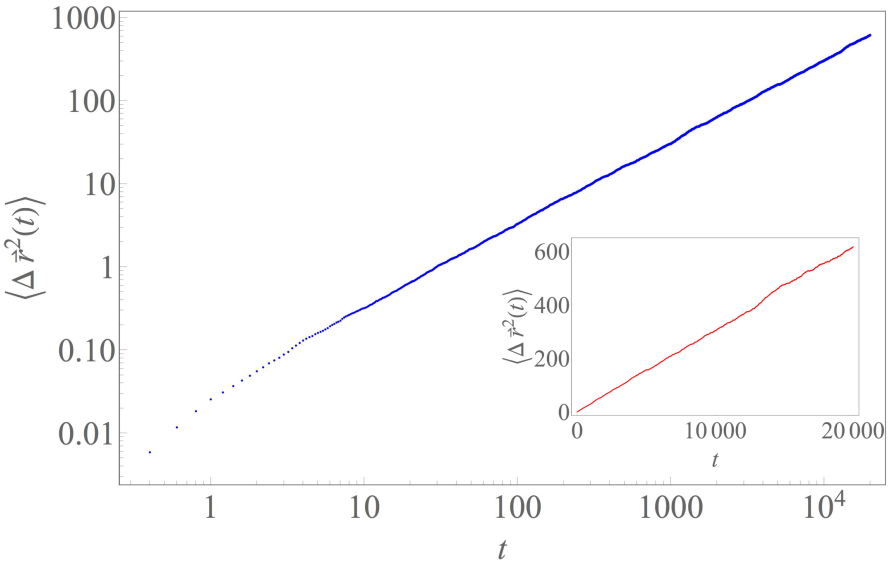

Figure 5.6: Mean square displacement for simulations performed considering passive Brownian particles, $\Delta t = 2 \times 10^{-2}$ and 20 000 as the total simulation time. The logarithmic scale is represented in blue and the linear scale in red.

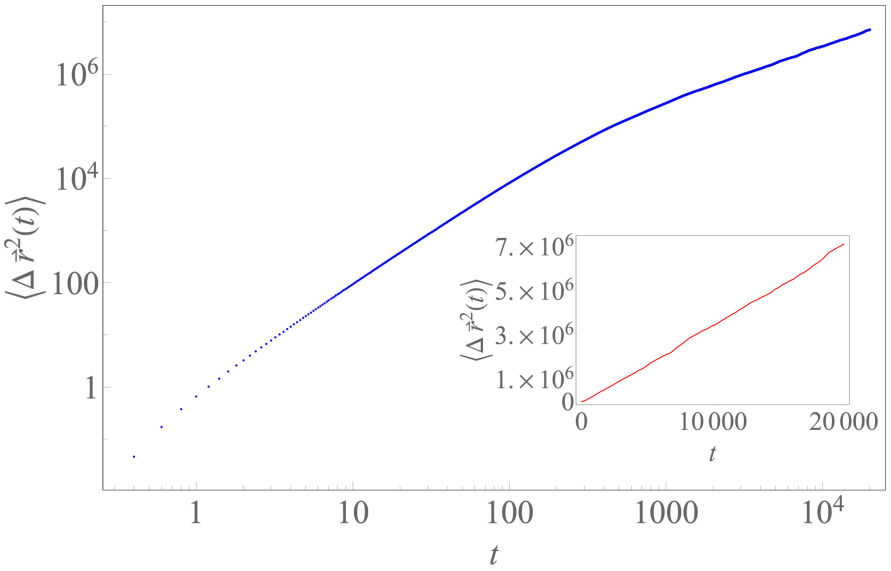

Figure 5.7: Mean square displacement for simulations performed considering active particles with $v_{drift} = 1$, $\Delta t = 2 \times 10^{-2}$ and 20 000 as the total simulation time. The logarithmic scale is represented in blue and the linear scale in red.

In Figure 5.6 we can again observe a linear dependence when considering passive Brownian particles

since when we calculated the slope of the line in $log\left(\left\langle \vec{r}^2(t)\right\rangle\right)$ *vs* $log(t)$ related to the case in Figure 5.6 the obtained value was 1.01 ± 0.03, which implies diffusive behaviour. For active particles, represented in Figure 5.7 we can observe two different types of behaviour: diffusive and ballistic. When we calculate the slopes of the lines in $log\left(\left\langle \vec{r}^2(t)\right\rangle\right)$ *vs* $log(t)$ we obtain a slope of 2.04 ± 0.05 for $t \leq 10^2$ and for $t > 10^3$ the slope is 1.01 ± 0.03. This means that, for an active particle, for times $t \leq 10^2$ the behaviour is ballistic and for times larger than 10^3 the behaviour is diffusive. Between these two times, 10^2 and 10^3, there is a transition from a ballistic behaviour to a diffusive behaviour.

Chapter 6

Interaction with a wall

Let us recall that we are considering a two-dimensional system. While in the previous chapter we considered periodic boundary conditions, here we will explicitly consider the presence of a solid wall. We analyse the effect of the wall for different suspending media, total simulation time and drift velocity in order to calculate the probability density function of the particles' position in each case.

6.1 Model for the wall

We are considering reflective boundary conditions, which means that everytime a particle tries to leave the box through a wall, it is reflected back as summarized in Figure 6.1.

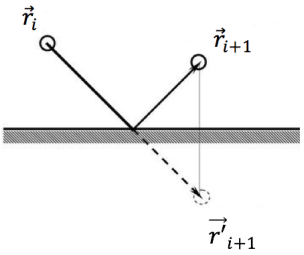

Figure 6.1: Reflective boundary conditions: if the particle is outside the box, then we consider a reflection of position vector across the line representing the wall. Source: adapted from [6]

Instead of PBC as was considered in the previous chapter, here we consider a square with lateral sides of length of L. We will consider the centre of this square at the point $(0,0)$, *i.e.* our system is the square defined by $\{(x,y) \in [-L/2, L/2] \times [-L/2, L/2]\}$ which is represented in Figure 6.2.

So, in each iteration n, we calculate the positions of each particle, *i.e.* the value of x_n and y_n of each particle. Applying reflective boundary conditions we impose that

- if $x_n > \frac{L}{2}$ then we assume that x_n is calculated as $x_n = L - x_n$,
- if $x_n < -\frac{L}{2}$ then we assume that x_n is calculated as $x_n = -L - x_n$,

and we assume the analogous conditions for the calculation of y_n.

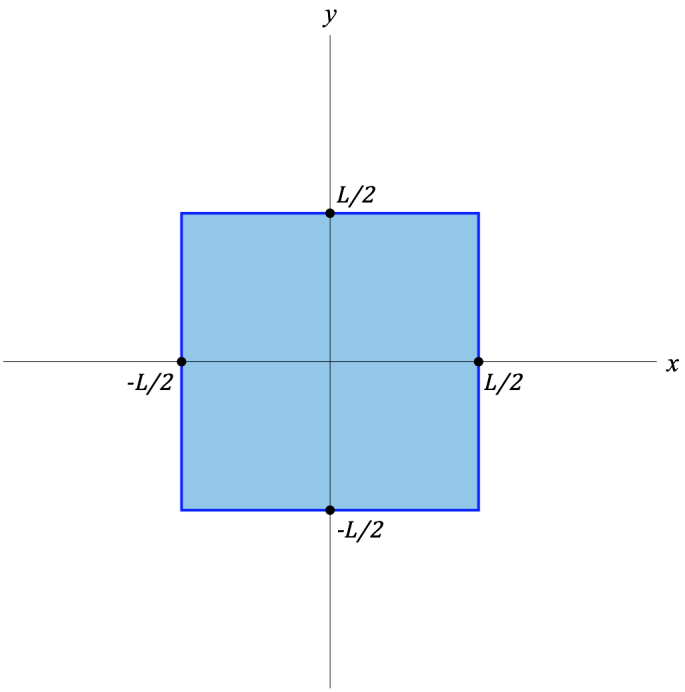

Figure 6.2: The walls of the system are represented by dark blue and the bulk is light blue.

6.2 Probability density function

6.2.1 Theory

Let ρ be a probability density function in which for an infinitely small dx, the quantity $\rho(x)dx$ represents the probability of finding a particle in the region centred in x which has length dx, where x is the position of the particle in x-axis.

And so here, $\rho(x)$ is such that

$$1 = \int_{-L/2}^{L/2} \rho(x)dx.$$

Now let us recall two known distributions: the uniform distribution and the normal distribution.

In a uniform distribution $U(-L/2, L/2)$ we have

$$\rho(x) = \frac{1}{L} \tag{6.1}$$

as it is represented in Figure 6.3a.

Thinking in a normal distribution $N(0,1)$ we can define a normalizing constant a and then we have

$$\rho(x) = ae^{-x^2/2}, \tag{6.2}$$

which is graphically represented by a Gaussian curve as in Figure 6.3b.

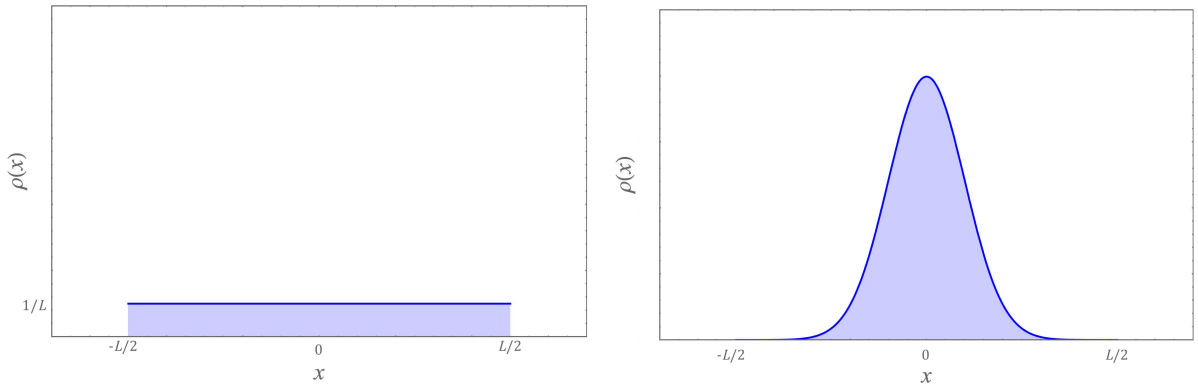

(a) (b)

Figure 6.3: Uniform (a) and normal (b) distributions represented, respectively, by equations 6.1 and 6.2 for $-L/2 \leq x \leq L/2$. The normal distribution here was assumed to have zero mean and unitary variance.

6.2.2 Numerical results

After having defined the probability density function and having recalled the definitions of uniform and normal distribution, we performed simulations of several particles in a square box in order to study the probability density function when considering different situations.

We performed simulations considering 10^3 particles in our square box, 10^3 samples and $\Delta t = min\{\frac{\tau_T}{2}, \frac{\tau_R}{2}\}$ (which in this case was 2.5), where $\tau_T = D_T^{-1}$ and $\tau_R = D_R^{-1}$ (which in this case we used the values $\tau_T = 5$ and $\tau_R = 6.7$). We chose this value for τ_T because in the individual motion of the particles there are two important time scales: the rotational and the translational scales. In the simulations, the time step sets the resolution of the numerical analysis. Since we want to describe both processes with some detail, as reference we use the smallest of these two characteristic times. Then, we divide by 2 to set the resolution referent to that time.

The value of each interval in the x-axis, Δx, is $\frac{\sqrt{D_T t_{total}}}{5}$, where t_{total} is the total simulation time, *i.e.* it is the product between Δt and the number of iterations in time. We chose this value for Δx because in the passive Brownian case, *i.e.* $v_{drift} = 0$, we have a Gaussian distribution with variance $D_T t_{total}$ and now we define that we want to see around 5 points (for example) in the area of interest of the peak.

In this model we do not consider interactions between the particles and we consider that the initial position of each particle coincides with the origin of the reference frame. Plus, we consider that initial velocity of each particle is zero.

The value of $\varphi(0)$ was obtained with a random number generator with uniform distribution between 0 and 2π.

Results with water at 20^o C

We started to perform simulations considering $L = 100$ as the length of the side of the square box. For simplicity, we supposed that the fluid that we were simulating in our square box was water at 20^o C.

Fixing the total simulation time to 2 500 and varying the value of v_{drift}, we observe that for passive Brownian particles the probability density function converges to a normal distribution as we can see in Figure 6.4a. For active particles we observe an accumulation of particles close to the walls and, also, this accumulation is higher for a larger value of drift velocity as we can observe from (b) to (e) of Figure 6.4 in which v_{drift} was, respectively, 0, 1, 2, 5 and 10.

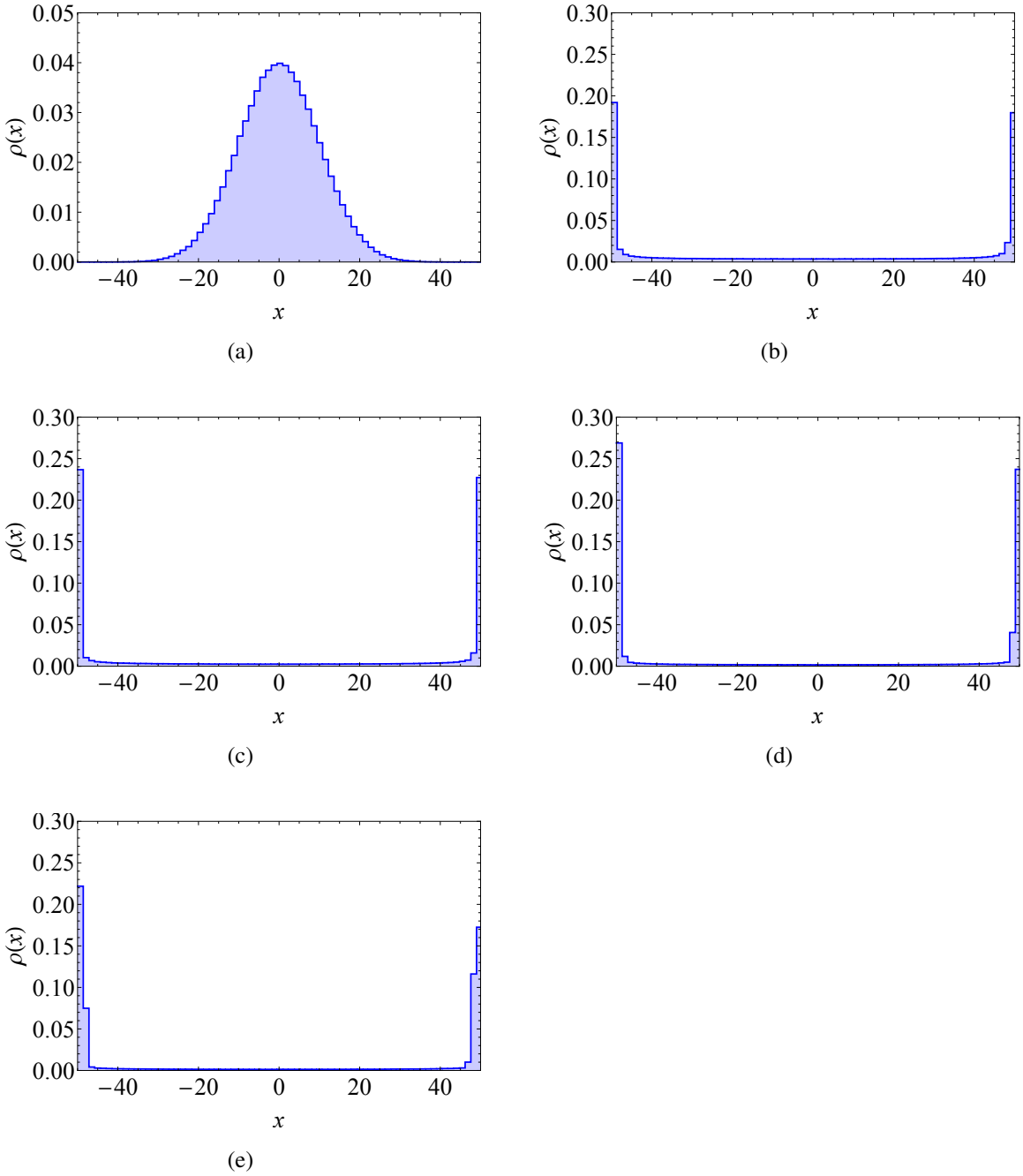

Figure 6.4: Probability density function of the particles for simulations performed considering different values for v_{drift} and total simulation time 2 500. In (a), (b), (c), (d) and (e) the value of v_{drift} was, respectively, 0, 1, 2, 5 and 10.

And what happens with the time evolution? To study the influence of time evolution in the probability density function, we studied the passive Brownian case, *i.e.* $v_{drift} = 0$, and two distinct active cases: one in which we considered $v_{drift} = 1$ and another with $v_{drift} = 5$. Again, we considered the same fluid, water at 20^o C, the same L, the same number of particles and samples and, also, the same time step. For passive Brownian particles, the probability density function converges over time from a normal distribution, as we can see from (a) to (d) of Figure 6.5, to a uniform distribution as we can see in Figure 6.5e.

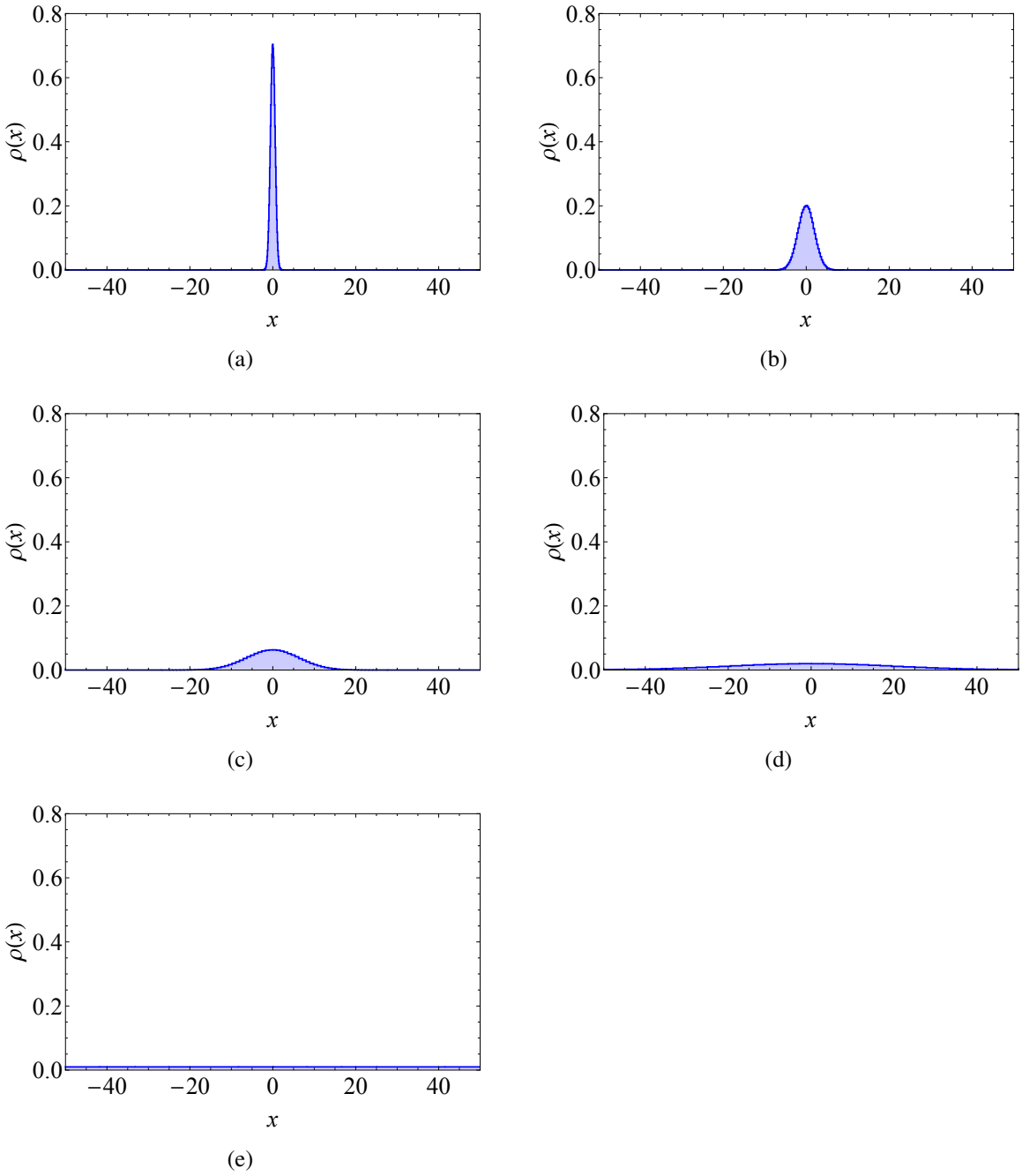

Figure 6.5: Probability density function of the particles for simulations done when considering passive Brownian particles in the system and different simulation times: 25 for (a), 250 for (b), 2 500 for (c), 25 000 for (d) and 250 000 for (e).

Now let us suppose an active case in which we consider $v_{drift} = 1$, *i.e.* all the particles in our system have $v_{drift} = 1$. Again, we considered the same fluid, water at 20^o C, the same L, the same number of particles and samples and, also, the same time step. In this case, we studied what happens to the probability density function for three different total simulation time: 25, 250 and 2 500. In this case, we observe a transition from a normal distribution, as we can see in Figure 6.6a, to a situation whereby there is accumulation of particles close to the walls, as we can see in Figure 6.6c.

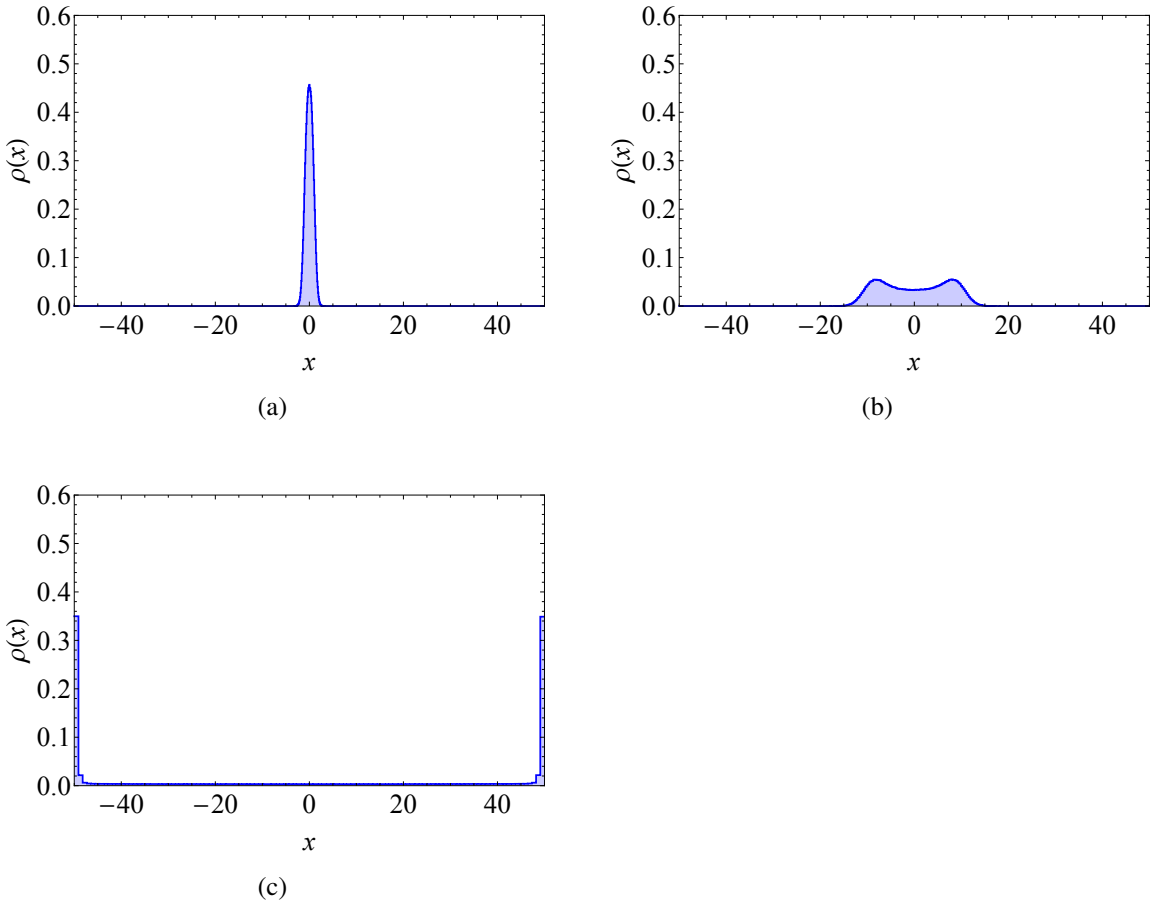

Figure 6.6: Probability density function of the particles for simulations when considering active particles with $v_{drift} = 1$ and different total simulation time: 25 for (a), 250 for (b) and 2 500 for (c).

Finally, we studied another active case but now we considered a larger value of drift velocity: $v_{drift} = 5$. Again, we considered the same fluid, water at 20^o C, the same L, the same number of particles and samples and, also, the same time step. The conclusions are the same as in the active case with $v_{drift} = 1$: there is a convergence from a normal distribution, as we can in Figure 6.7a, to a situation in which there is accumulation of particles close to the walls, as we can see in Figure 6.7c.

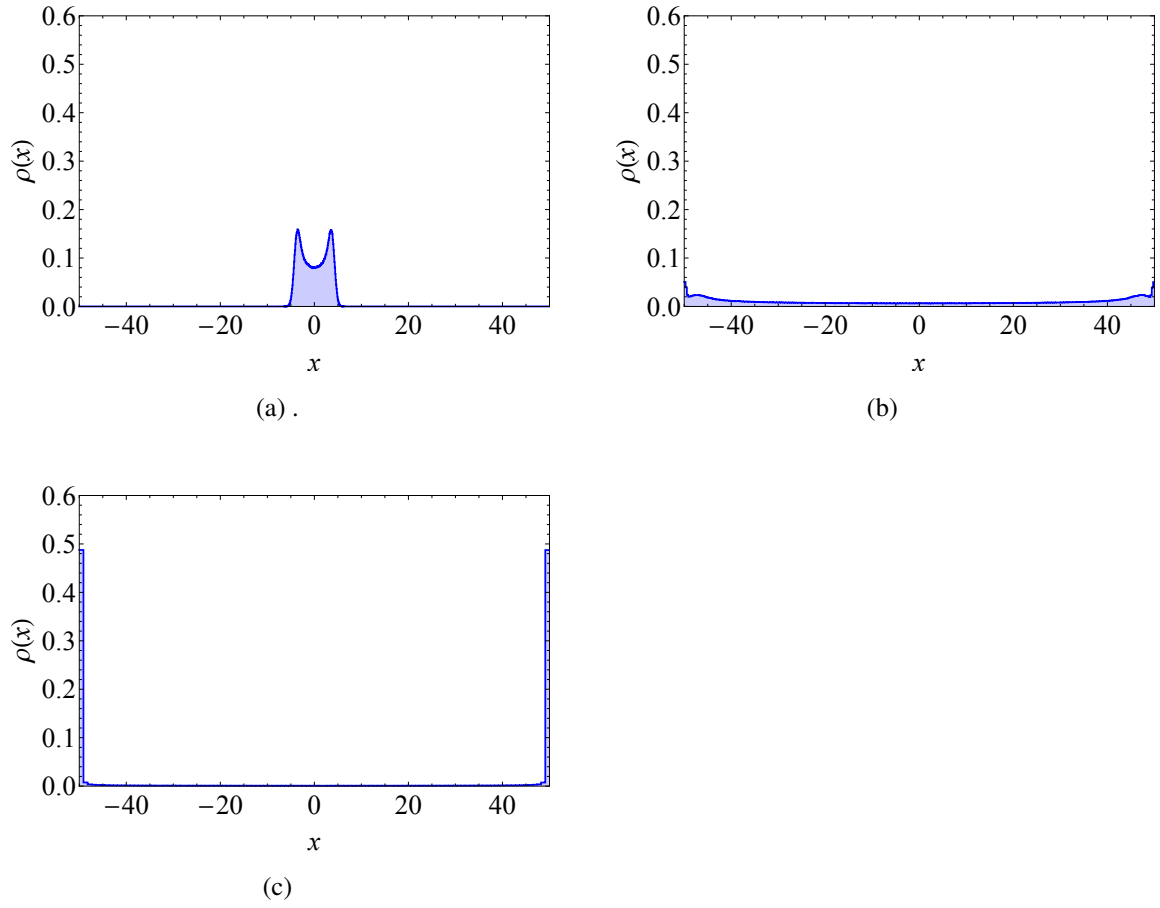

Figure 6.7: Probability density function of the particles for simulations when considering active particles with $v_{drift} = 5$ and different total simulation times: 25 for (a), 250 for (b) and 2 500 for (c).

When comparing the two previous distinct active cases, in which we considered $v_{drift} = 1$ and $v_{drift} = 5$, we can draw an interesting conclusion. In Figures 6.6c and 6.7c we observe an accumulation of particles near the wall, meaning that there is accumulation of particles close to the walls after the same total simulation time when considering $v_{drift} = 1$ and $v_{drift} = 5$. Now, if we compare Figures 6.6a and 6.7a, we see that the accumulation near the walls is faster for the largest v_{drift} as we can confirm by comparing Figures 6.6c and 6.7c since the value of the probability density function is larger near the walls in the last case.

Comparing different fluids

After studying the probability density function for the case of water at 20^oC when considering different values of drift velocity and different total simulation times, we compared what happens when we consider different values of drift velocity and different total simulation times and four different fluids. The chosen fluids were: water at 20^oC, water at 100^o C, blood at 37^o C and olive oil at 20^o C. These fluids have different viscosities and so, by Stokes-Einstein equation, their diffusion coefficient is different. For water at 20^oC, water at 100^o C, blood at 37^o C and olive oil at 20^o C the diffusion coefficient is, respectively, 0.2, 1, 6.5×10^{-2} and 2×10^{-3}, in simulation units.

Our simulations were performed considering $L = 100$, 10^3 particles, 10^3 samples and the minimum value of $\Delta t = min\{\frac{\tau_T}{2}, \frac{\tau_R}{2}\}$ between the four liquids, where $\tau_T = D_T^{-1}$ and $\tau_R = D_R^{-1}$, which in this case was $\Delta t = 0.5$.

The value of each interval in the x-axis, Δx, is the minimum value of $\frac{\sqrt{t_{total} D_T}}{5}$ between the four liquids, where t_{total} is the product between Δt and the number of iterations in time.

For the passive Brownian case, we observe what happens to the probability density function for each fluid over time in Figure 6.8. There is convergence of all curves to a smoother curve and the maximum value of the probability density function decreases over time.

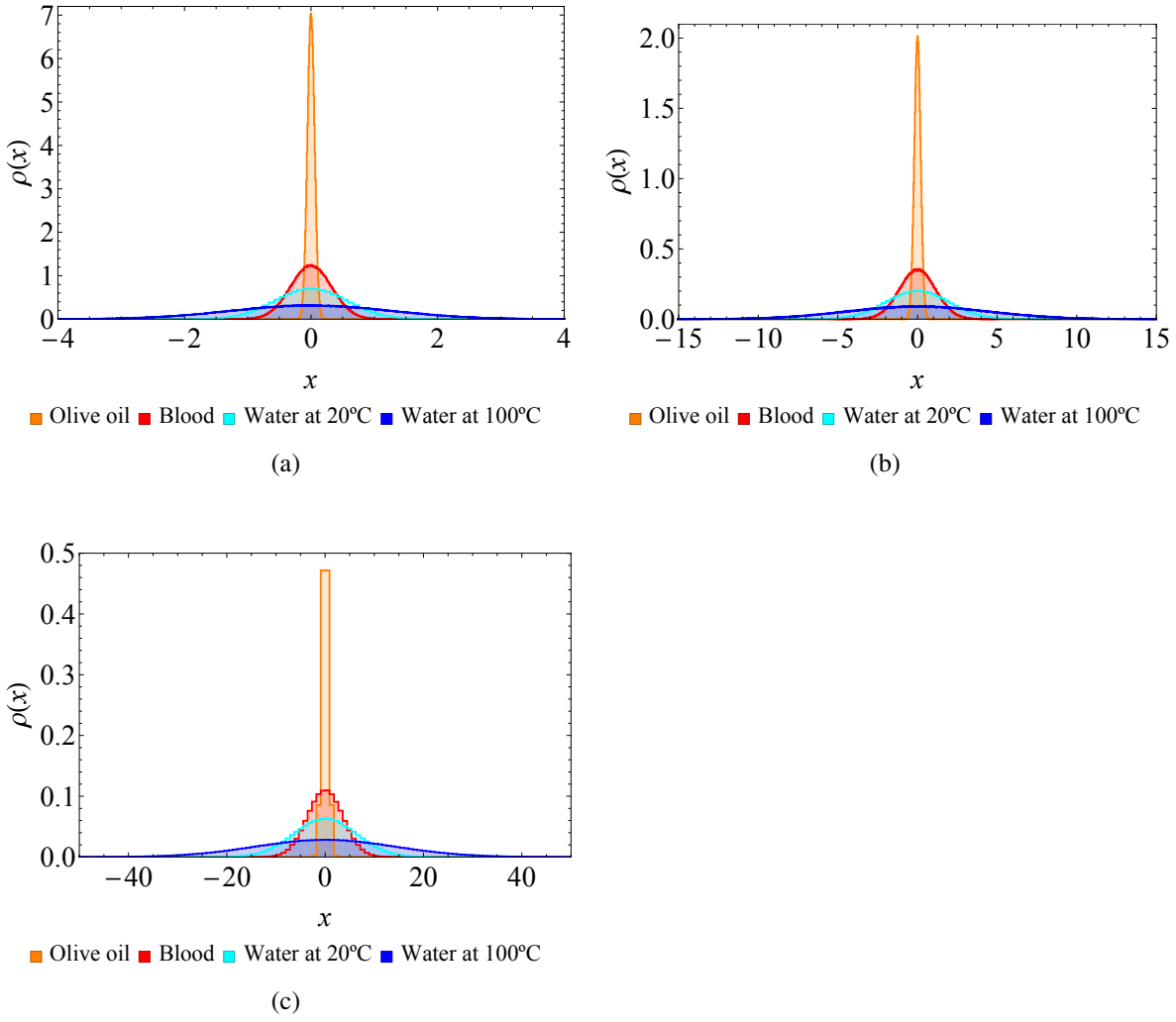

Figure 6.8: Probability density function of the particles for simulations with passive Brownian particles and different total simulation times: 2, 20 and 200 for (a), (b) and (c), respectively.

Then we considered an active case in which $v_{drift} = 1$, *i.e.* all the particles in our system have $v_{drift} = 1$. Again, we considered the same fluids, the same L, the same number of particles and samples and, also, the same time step. Here, we studied what happens to the probability density function for three different total simulation time: 2, 20 and 200. In this active case, we can see that there is a convergence over time to a state in which there is an accumulation of particles close to the walls, as we can see in Figure 6.9c.

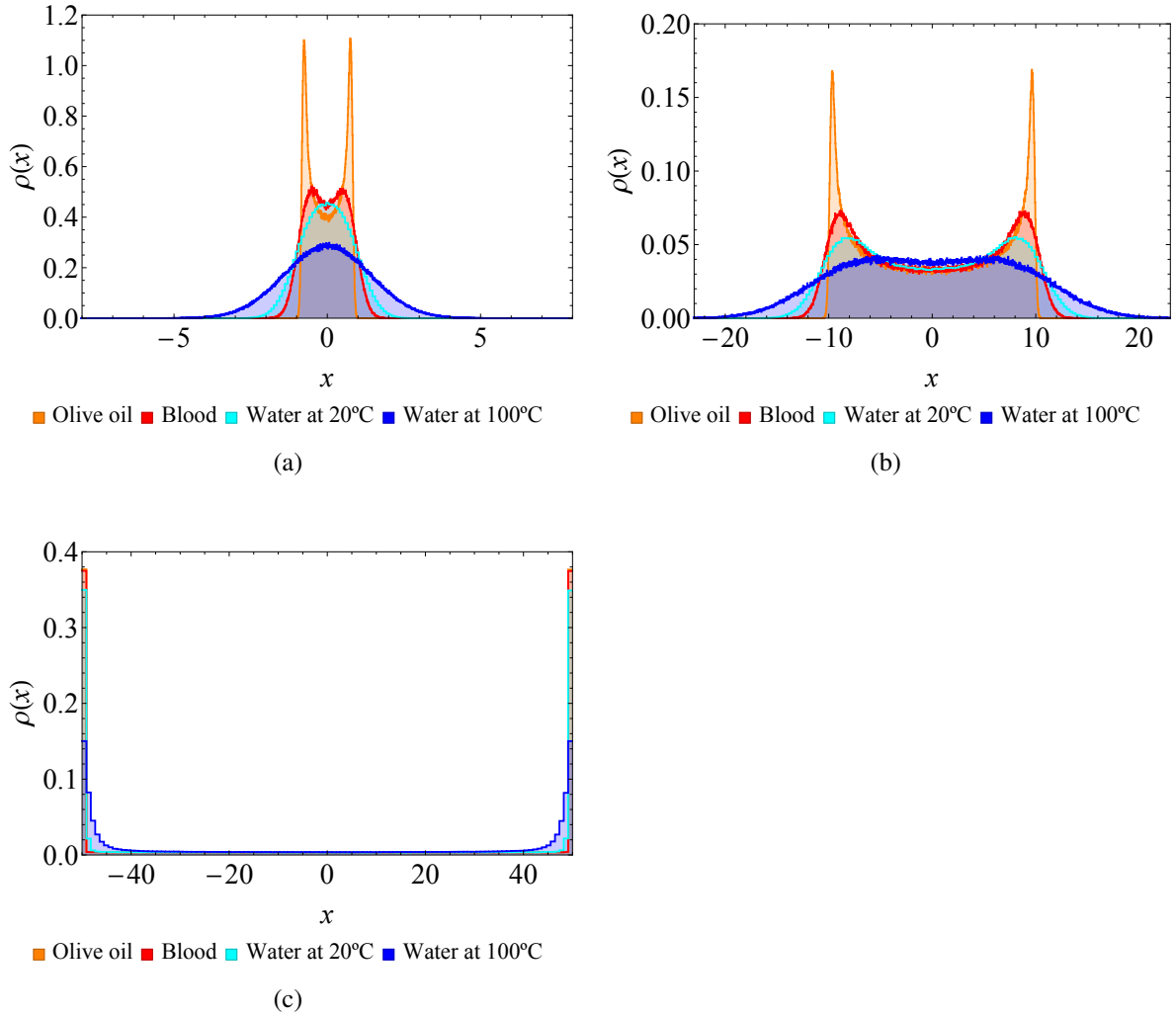

Figure 6.9: Probability density function of the particles for simulations with $v_{drift} = 1$ and different total simulation times: 2, 20 and 200 for (a), (b) and (c), respectively.

The last case studied was another active case in which we considered a larger value of drift velocity: $v_{drift} = 5$. Again, we considered the same fluids, the same L, the same number of particles and samples and, also, the same time step. Our conclusion for this case is the same as for the active case in which $v_{drift} = 1$: a convergence occurs over time to a state in which there is an accumulation of particles close to the walls, as we can see in Figure 6.10c.

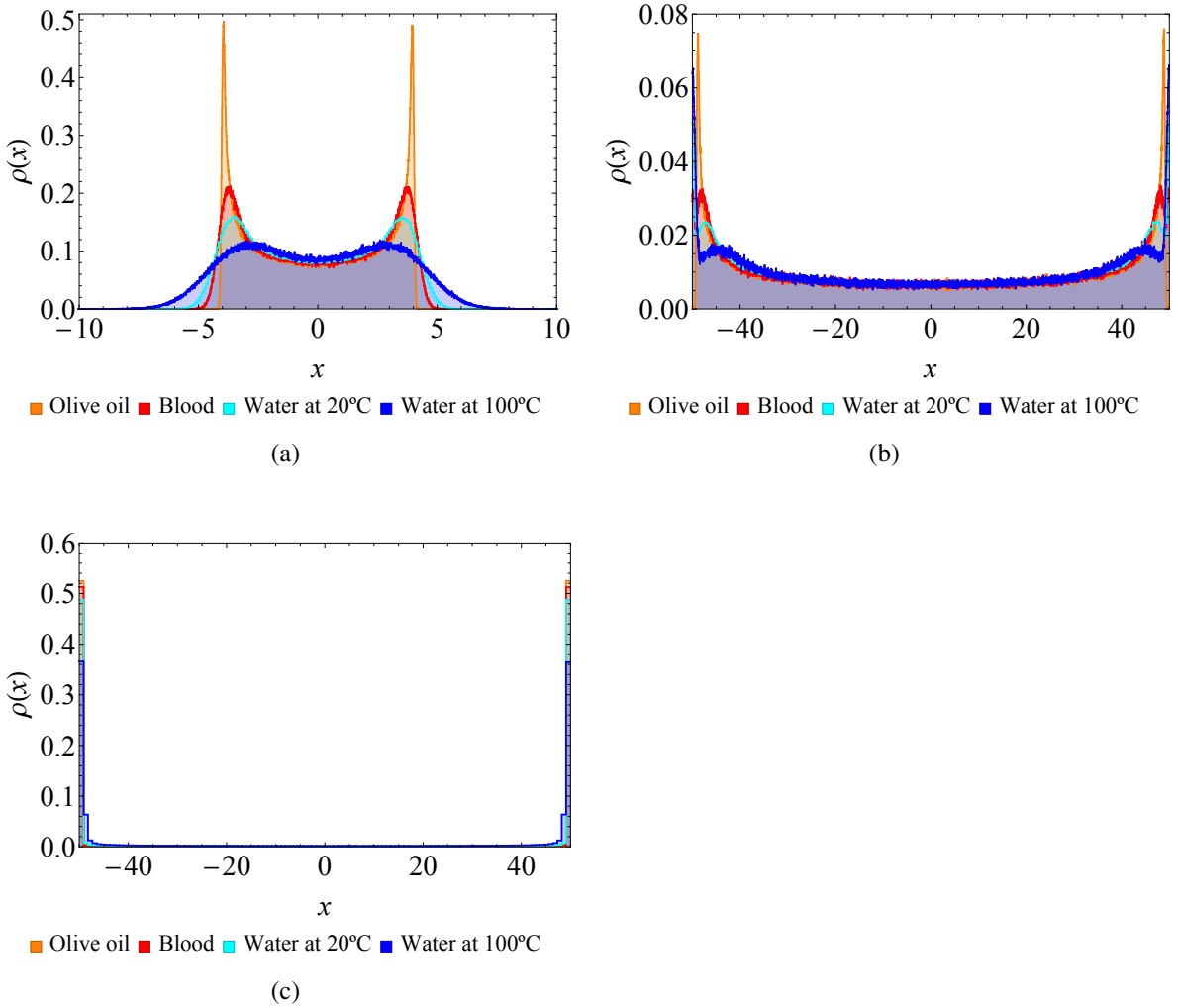

Figure 6.10: Probability density function of the particles for simulations with $v_{drift} = 5$ and different total simulation times: 2, 20 and 200 for (a), (b) and (c), respectively.

In each distinct active case, *i.e.* when $v_{drift} = 1$ or $v_{drift} = 5$, we can observe that for a longer total simulation time, we have a higher probability density of particles near the walls as we can see in Figures 6.9 and 6.10.

For a fixed total simulation time, we can observe that, for a larger value of v_{drift}, we will have a higher probability density of particles near the wall once particle accumulation has occurred, and this probability density increases when the value of D_T decreases. This is interesting, as the first active particles to reach the boundary in simulations are those in the medium with the largest D_T (see figures 6.9a and 6.10a), but these will not have the highest peak at the boundary once boundary accumulation in all four mediums has occurred. What is happening is that when the particles in a larger D_T medium periodically leave the boundary, they will travel further before returning to the boundary (larger D_T) and they will also leave the boundary more often (because of the relation between D_T and D_R). This leads to a wider accumulation band and therefore a lower value in the probability density function right at the

boundary.

Chapter 7

Interaction between particles

So far we have considered non-interacting particles. In this chapter we will study the role of interactions.

As in the previous chapter, here we also consider the existence of a wall.

We will study two different models, A and B, in order to model the interactions between particles with different potentials. We will start with a model (A), where the interaction is purely repulsive and then a model (B) where the interaction is the superposition of a repulsive and an attractive term.

7.1 Model A

7.1.1 Theory

The potential considered here is

$$V_A(r) = \lambda \cdot exp\left(-\frac{r}{\sigma_A}\right), \tag{7.1}$$

where:

- r is the length of the vector $\vec{r}(t) := (x(t), y(t))$; $r \in \mathbb{R}_0^+$;
- λ is the amplitude: $\lambda \in \mathbb{R}_0^+$ and it is units of energy;
- σ_A establishes a length scale: $\sigma_A \in \mathbb{R}_0^+$.

Since the associated potential is time independent, the force is conservative and it is given by $\vec{F}(r) = -\vec{\nabla}V(r)$. Then, in this model the force that a particle exerts on other is given by

$$\vec{F}_A(r) = \frac{\lambda}{\sigma_A} exp\left(-\frac{r}{\sigma_A}\right)\vec{u}_{\vec{r}}, \tag{7.2}$$

where $\vec{u}_{\vec{r}} = \frac{\vec{r}}{r}$.

Then our new system of equations is given by

$$\begin{cases} \dot{\vec{r}}(t) = \vec{v}(t) \\ 0 = -\gamma\vec{v}(t) + \vec{\xi}(t) + \vec{F^T}(t) + \vec{F}_A(t)\,. \\ \dot{\varphi}(t) = \xi_\varphi(t) \end{cases} \tag{7.3}$$

7.1.2 Numerical implementation

Supposing we have N_p particles in our system, if we calculate the interactions between all the particles, we would need to calculate $\frac{N_p(N_p-1)}{2}$ interactions. We can reduce the number of calculations by setting a cut-off distance in our potential.

For the numerical implementation of this model, we consider a cut-off distance, r_c, and then, numerically we have

$$V_A^{trunc}(r) = \begin{cases} \lambda \cdot exp\left(-\frac{r}{\sigma_A}\right) - \lambda \cdot exp\left(-\frac{r_c}{\sigma_A}\right) & \text{if } r \leqslant r_c \\ 0 & \text{if } r > r_c \end{cases} \tag{7.4}$$

and so

$$\vec{F}_A^{trunc}(r) = \begin{cases} \left[\frac{\lambda}{\sigma_A} exp\left(-\frac{r}{\sigma_A}\right) - \frac{\lambda}{\sigma_A} exp\left(-\frac{r_c}{\sigma_A}\right)\right] \vec{u}_{\vec{r}} & \text{if } r \leqslant r_c \\ \vec{0} & \text{if } r > r_c \end{cases}. \tag{7.5}$$

It can be easily verified that $V_A^{trunc}(r_c) = 0$, thus eliminating the discontinuity jump at $r = r_c$.

Here, we will define **radius** as half of σ_A. In our simulations we use $\sigma_A = 1$, setting the units of length.

Then we need to define the cut-off distance, r_c, and, since the function $V_A(r)$ is a strictly decreasing function we assume a minimum value for the potential in which the corresponding distance is the cut-off distance.

To set a value for minimum of the potential, we set $k_BT = 1$ and then the potential is given in units of k_BT. If we then multiply the potential by a pre-factor of 0.1 this implies that the energy of interaction is about 10% of the thermal energy. So, we consider that the interaction between the particles is negligible when it is compared with the thermal energy. A remark regarding the pre-factor: we know that 1% or even 0.1% would be better choices for this pre-factor, but since we need to take into account the precision and the time of simulation we need to choose a reasonable value, such as 10%. So, we assume that the minimum value for the potential is $V(r_c) = 0.1\lambda$ and so $r_c = \sigma_A log\,(10)$.

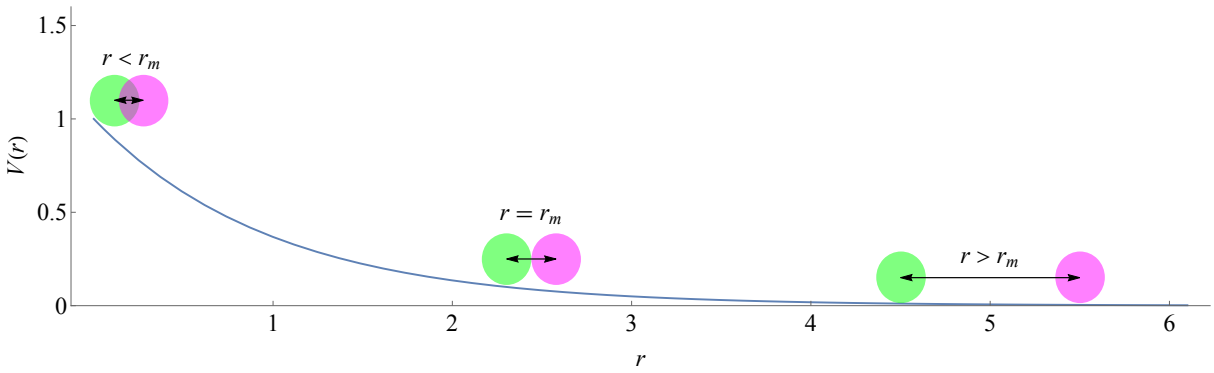

Figure 7.1: Example of potential from model A represented for three distinct distances between particles: $r < r_m$, $r = r_m$ and $r > r_m$ where $r_m = 2\sigma_A$. When $r = r_m$ we have our radius defined meaning that two particles are tangent to each other.

A note about the chosen time step

Before we show the results obtained with our simulations, we should include a small remark here about the choice of the value of the time step for these simulations.

We decided to set $\lambda = 1$ to define the energy scale and $\sigma_A = 1$.

And now, one can ask, how to choose the time step of our simulations?

We need to choose a time resolution in which one can observe diffusion of particles.

Let us give two "bad" examples: one with too small a time step and the other with too large a time step.

We performed simulations considering model A and $L = 20$. In these simulations, we considered two passive Brownian particles with initial positions $(-0.5, 0)$ and $(0.5, 0)$ and with initial velocity $\vec{u}_x$ and $-\vec{u}_x$, respectively. The following results are referent to these two situations.

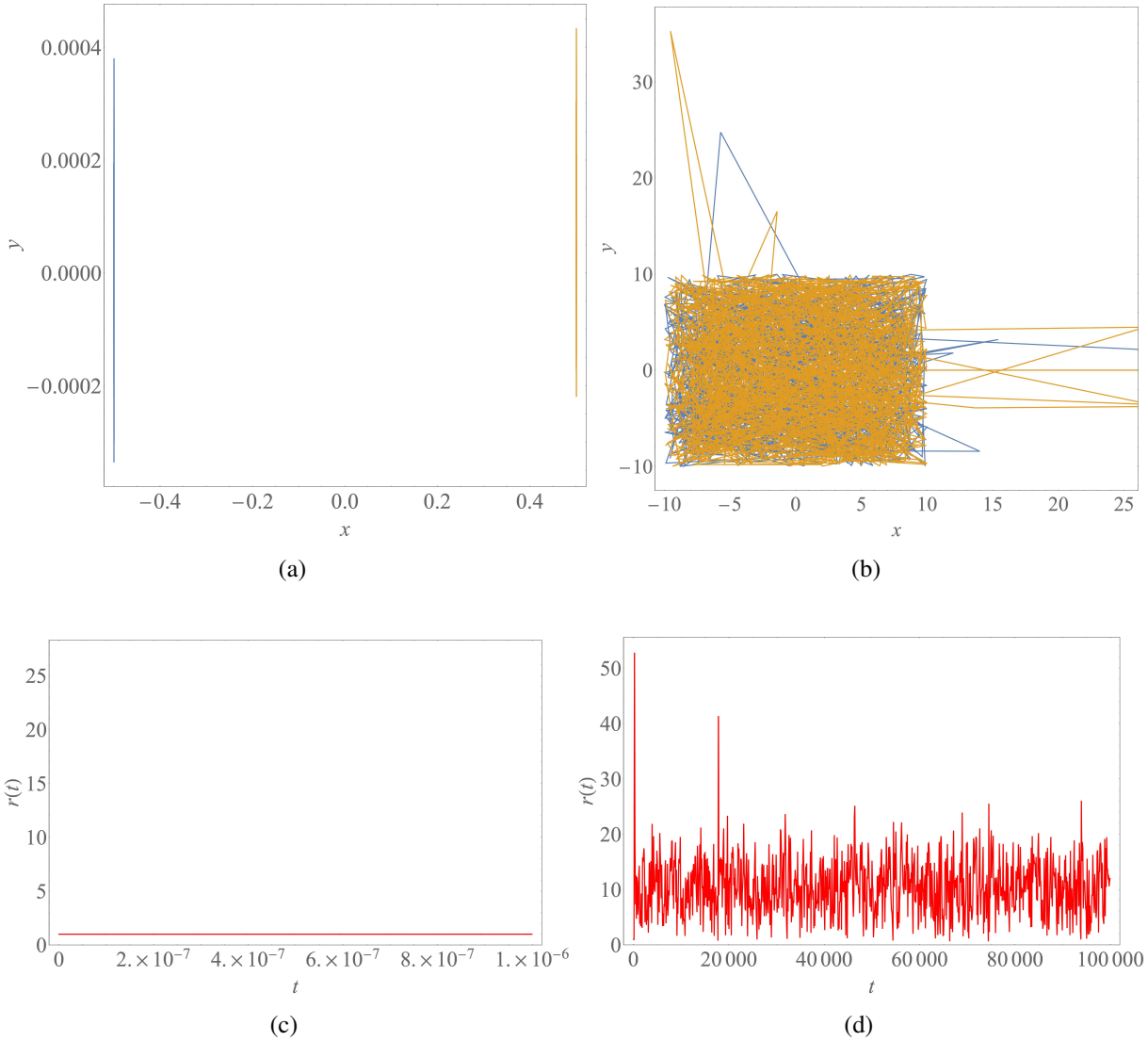

Figure 7.2: Interaction between two particles with model A considering two different time steps and 10^3 iterations. In (a) and (b) it is represented the trajectory of two particles, one in blue and another in orange, when considering $\Delta t = 10^{-9}$ and $\Delta t = 10^2$, respectively. In (c) and (d) the distance between the particles over time is represented when considering $\Delta t = 10^{-9}$ and $\Delta t = 10^2$, respectively.

We started by setting $\Delta t = 10^{-9}$ and then we did simulations for 10^3 iterations. In Figure 7.2a we can see that displacement of both particles it was very small and then if we look at Figure 7.2c we can verify

that the distance between them was approximately constant throughout the simulation. So, we conclude that such a small time step, $\Delta t = 10^{-9}$, is not suited for our studies.

We can think in the same way but now with a much larger time step. Defining $\Delta t = 10^2$ and with simulations with 10^3 iterations in time, we obtained the results of Figures 7.2b and 7.2d. Let us recall that $L = 20$, so we have a square box as it was defined in Figure 6.2. Then, what we observe in Figure 7.2b is clearly wrong since the trajectory of the particles intersects the area outside the box. This can also be seen in Figure 7.2d because the maximum distance between the particles is $20\sqrt{2}$ and looking at the figure we see that $r(t)$ reaches a maximum value which is larger than 50. This occurs because if we integrate numerically the position and the velocity using a very large time step, the obtained values would be very large.

This is enough to conclude that we need a suitable value for the time step so that none of the last two situations happen.

Interaction between two particles

In these simulations we used $\sigma_A = 1$ meaning each particle has radius $R = 0.5$ and the cut-off distance is $log\,(10)$. We considered $\Delta t = 10^{-4}$ and we performed 10^6 iterations in time. For the length of the square box we considered $L = 20$. In order to study the difference between the passive Brownian and the active case, we considered two particles with initial positions $(-R,0)$ and $(R,0)$ and with initial velocity $\vec{u}_x$ and $-\vec{u}_x$, respectively.

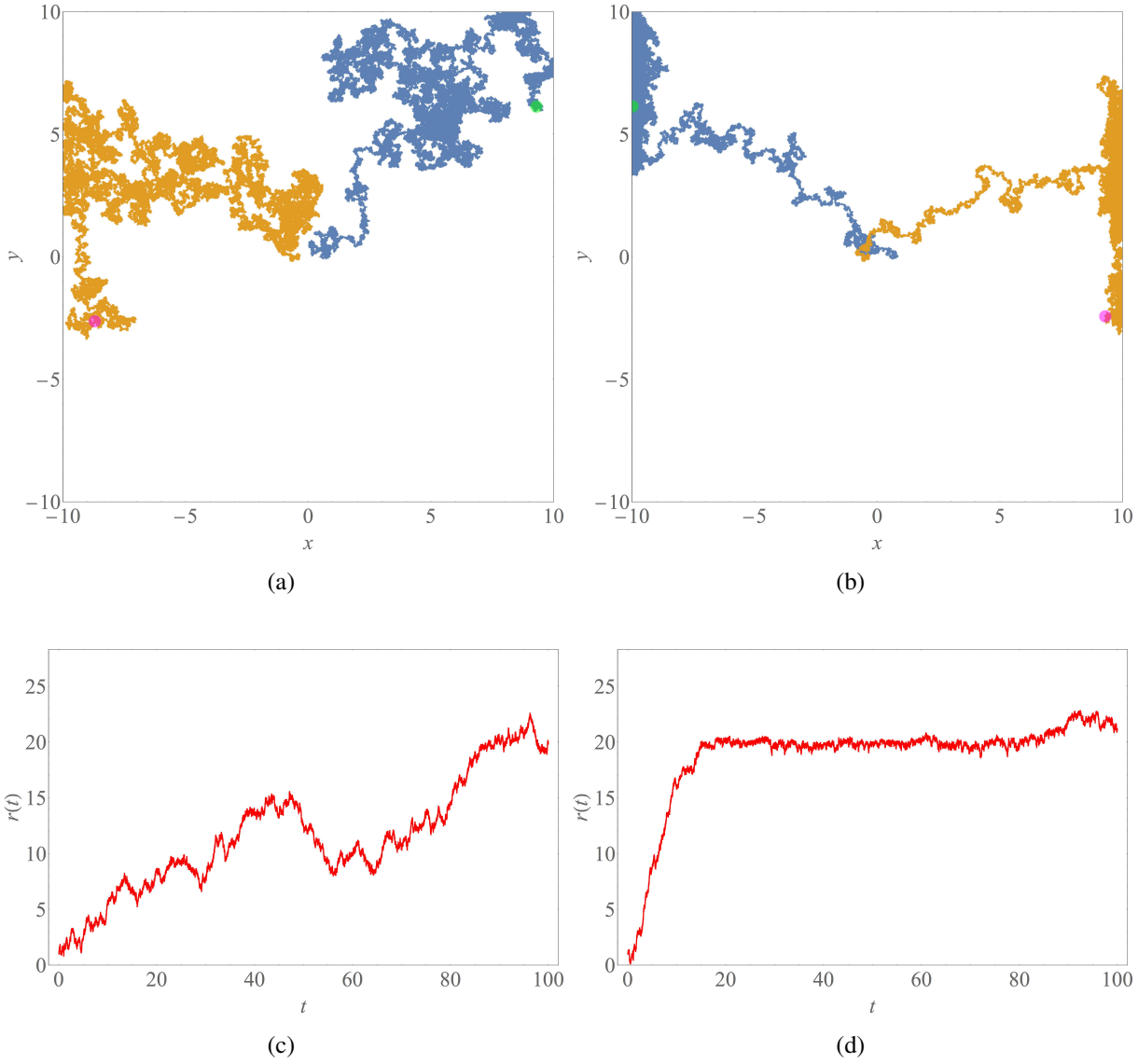

Figure 7.3: Interaction between two particles with model A when considering two passive Brownian particles, (a) and (c), or two active particles with drift velocity of $v_{drift} = 1$, (b) and (d). The initial positions for the particles are $(-R,0)$ and $(R,0)$ with initial velocity $\vec{u}_x$ and $-\vec{u}_x$, respectively. In (a) and (b) the trajectory of each particle is represented: one in orange and another in blue. The magenta and green dots represent the final positions of the orange and blue particles respectively. In (c) and (d) the distance between the two particles over time is represented.

In Figure 7.3a we see the trajectory of two passive Brownian particles where the magenta and green dots represent the final position of the particles with initial position $(-R,0)$ and $(R,0)$, respectively. In Figure 7.3c we can see a plot of the distance between the particles, $r(t)$, as function of time, t, in which we see that the particles start to move away from each other and when the cut-off distance is reached, *i.e.* $r(t) = r_c \approx 2.303$, there are no external forces acting in each particle, so the potential is not playing

a role. After $t = 40$ we see that the distance between the particles starts to decrease and so they begin to approximate and this is due to the absence of particle-particle interactions.

Now let us see the difference with a case in which we have two active particles with drift velocity of $v_{drift} = 1$. In Figure 7.3b we see the trajectory of two active particles where the magenta and green dots represent the final position of the particles with initial position $(-R,0)$ and $(R,0)$, respectively. In Figure 7.3c we can see the plot of the distance between the two particles, $r(t)$, as function of time, t. In this figure we see that in the beginning the particles start to move away from each other as in the previous case but then the distance between them tends to stabilize. This is due to the repulsive nature of the potential and also to the fact of having a non-zero value for v_{drift}. Moreover, the existence of the walls contributes for this stabilization of the distance between particles.

Interaction between several particles

Here, we considered more than two particles to study the probability density function of this model with different values of v_{drift}. The simulations were performed with $L = 20$, $\lambda = 1$, $\sigma_A = 1$, 10^2 particles, 10^3 samples, $\Delta t = 0.1$, $D_T = 0.2$ and different values of v_{drift}.

Firstly, we performed simulations with passive Brownian particles.

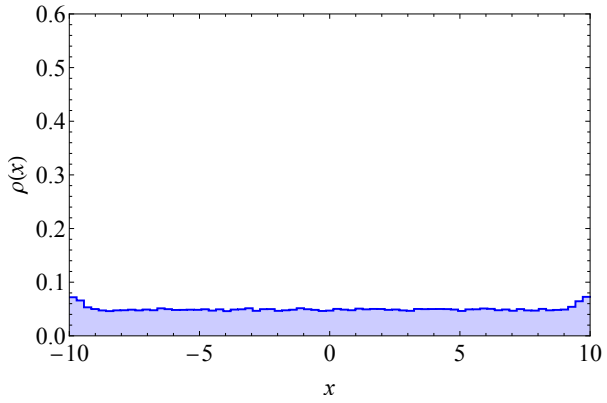

Figure 7.4: Probability density function of passive Brownian particle when considering a total simulation time of 10^2.

In Figure 7.4 we can see the probability density function of passive Brownian particles for a total simulation time of 10^2. In this figure we can see that the probability density function is not quite uniform, this is due to fluctuations of the simulations. We ran simulations with longer total simulation times to confirm that the probability density function became uniform.

And what happens if we consider an active case?

Besides the changing the drift velocity value to $v_{drift} = 1$, we considered the same conditions in order to obtain these plots: $L = 20$, 10^2 particles, 10^3 samples and three different simulation times (1, 10 and 10^2 time units for Figures 7.5a, 7.5b and 7.5c respectively).

In Figure 7.5a we can see some accumulation of particles near the walls and in Figures 7.5b and 7.5c we can clearly observe a strong accumulation of particles near the walls when comparing with the bulk.

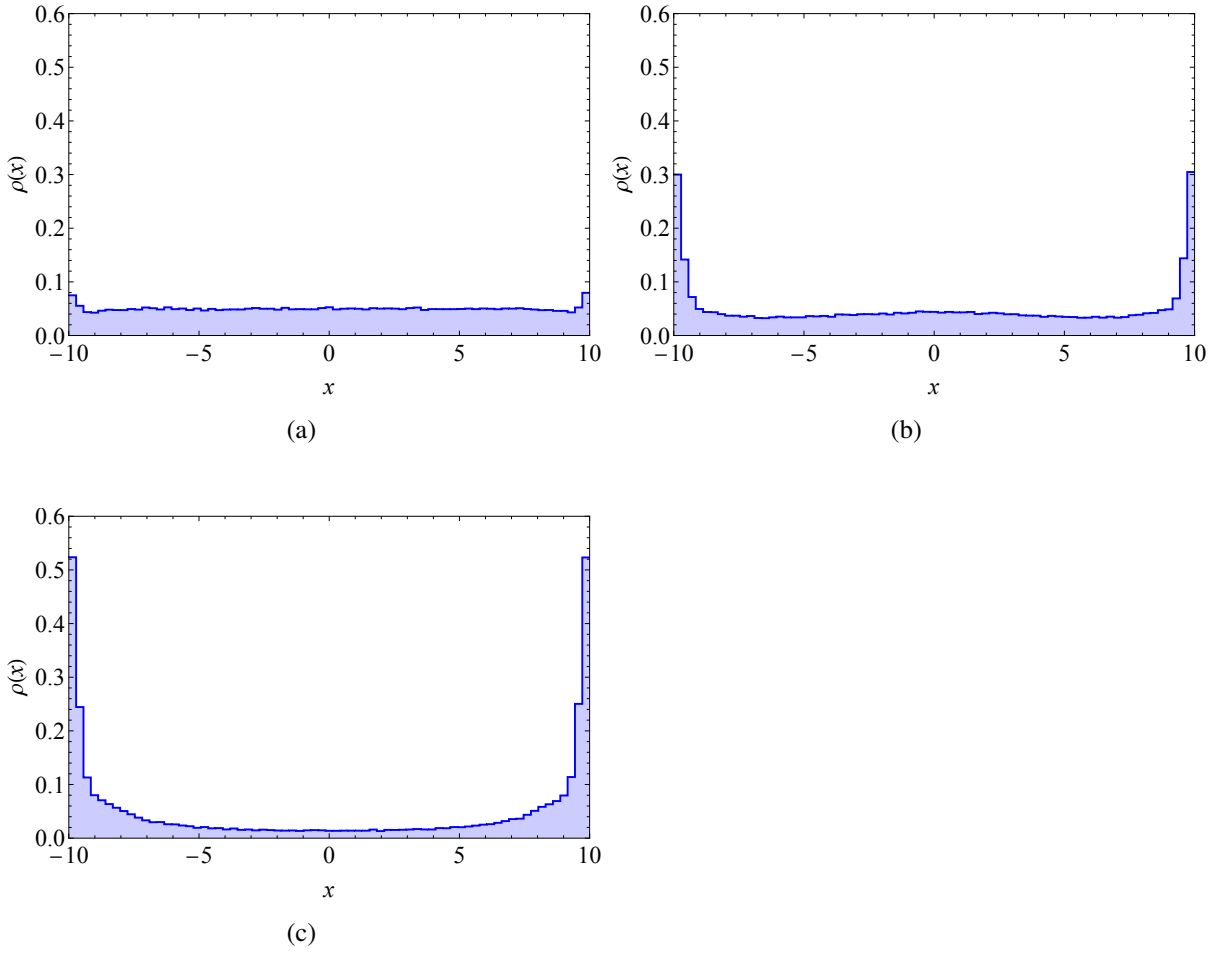

Figure 7.5: Probability density function of active particles considering $v_{drift} = 1$ and different total simulation time: 1, 10 and 10^2 for (a), (b) and (c), respectively.

And now, what if we have an even larger value of v_{drift}? Let us consider $v_{drift} = 5$.

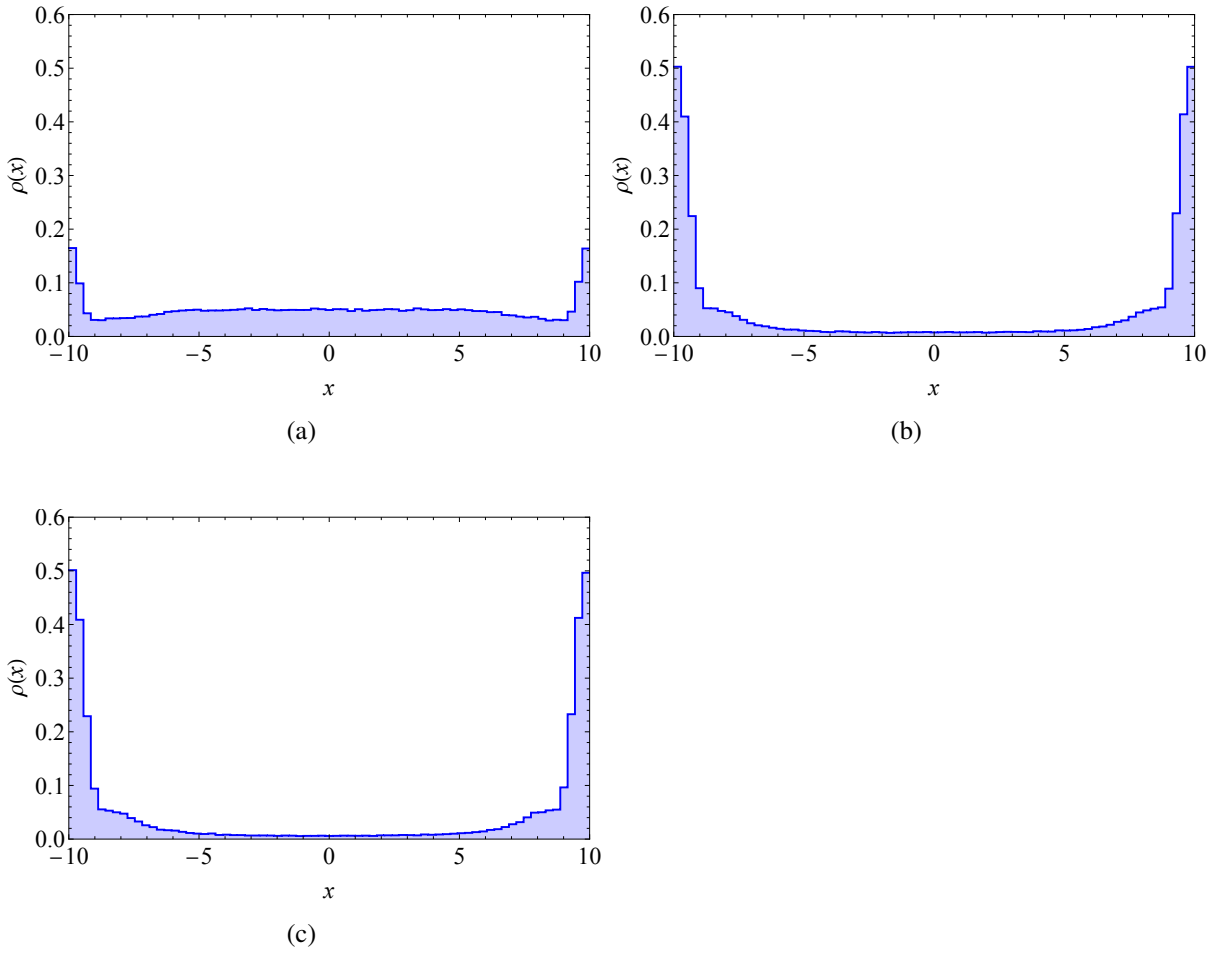

Figure 7.6: Probability density function of active particles considering $v_{drift} = 5$ and different total simulation times: 1, 10 and 10^2 for (a), (b) and (c), respectively.

Again, we considered the same conditions as before, with exception of v_{drift}. So, here we have $v_{drift} = 5$, $L = 20$, 10^2 particles, 10^3 samples and different total simulation times: 1, 10 and 10^2.

As in the previous case, where $v_{drift} = 1$, we can verify that in Figure 7.6a the particles are starting to accumulate near the walls but there is still an amount of particles in the bulk. In Figures 7.6b and 7.6c we can see that in the centre of the bulk the probability density function tends to zero whereas near the walls it has increased when compared with the case of Figure 7.6a.

When comparing Figures 7.5b and 7.6b, which represent the probability density function for the same total simulation time, 10, and different values of v_{drift} (1 and 5 respectively) we can observe that in Figure 7.5b, $\rho(x)$ reaches a maximum value of, approximately, 0.3 while in Figure 7.6b this maximum value is now, approximately, 0.5. If we then look at Figure 7.5c, in which $v_{drift} = 1$ and the total simulation time is 10^2, we see that $\rho(x)$ reaches a maximum value of, approximately, 0.55. This leads us to conclude that with a larger value of v_{drift}, the particles take less time to accumulate near the walls.

7.2 Model B

7.2.1 Theory

Here, we consider a potential which is repulsive for short distances and attractive for long distances. So, this potential is more complex than the one studied in model A.

The potential considered is the Lennard-Jones potential, which is given by

$$V_B(r) = \varepsilon \left[\left(\frac{\sigma_B}{r} \right)^{12} - \left(\frac{\sigma_B}{r} \right)^{6} \right], \tag{7.6}$$

where:

- r is the length of the vector $\vec{r}(t)$: $r \in \mathbb{R}_0^+$;
- ε is the motion amplitude which defines the strength of the interaction: $\varepsilon \in \mathbb{R}_0^+$;
- σ_B establishes a length scale: $\sigma_B \in \mathbb{R}_0^+$.

The force $\vec{F}$ is given by $\vec{F}(r) = -\vec{\nabla} V(r)$, so

$$F_B(r) = 6\frac{\varepsilon}{r} \left[2\left(\frac{\sigma_B}{r} \right)^{12} - \left(\frac{\sigma_B}{r} \right)^{6} \right] \vec{u}_{\vec{r}}, \tag{7.7}$$

where $\vec{u}_{\vec{r}} = \frac{\vec{r}}{r}$.

Then our new system of equations is given by

$$\begin{cases} \dot{\vec{r}}(t) = \vec{v}(t) \\ 0 = -\gamma \vec{v}(t) + \vec{\xi}(t) + \vec{F^T}(t) + \vec{F}_B(t) \\ \dot{\varphi}(t) = \xi_\varphi(t) \end{cases}. \tag{7.8}$$

7.2.2 Numerical implementation

Here, we will define **radius** as half of the distance between the centres of two neighbouring particles when the potential reaches its minimum value. Denoting r_m by the value of r where the potential is minimum, we obtain $r_m = \sigma_B 2^{1/6}$.

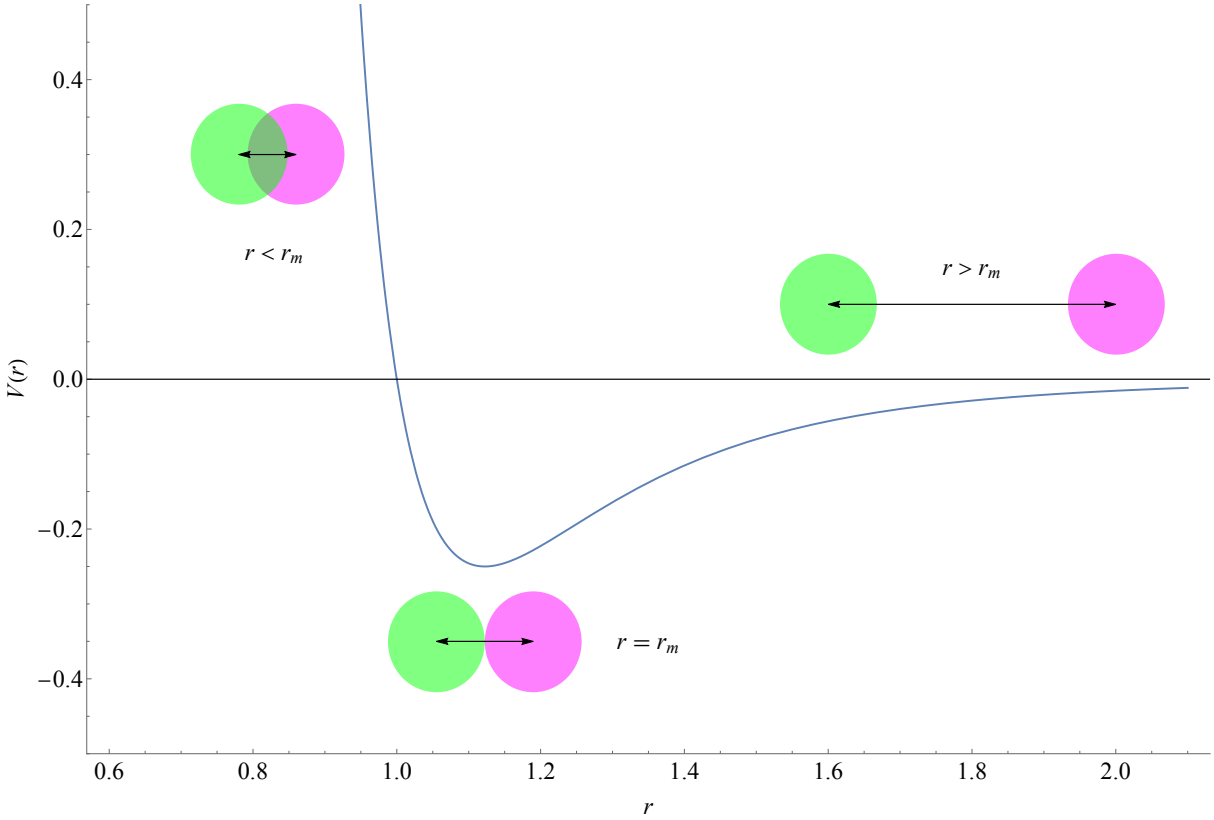

Figure 7.7: Definition of radius: we define radius as half of the distance r_m.

In our simulations, we used the reduced units for all the parameters, *i.e.* $\varepsilon = \sigma_B = 1$. [14]

For the numerical implementation of this model and by the same reasons as it was explained for model B (reduce the number of calculations), we consider a cut-off distance, r_c, defined by $r_c = 2.5\sigma_B$ and then, numerically we have

$$V_B^{trunc}(r) = \begin{cases} \varepsilon\left[\left(\frac{\sigma_B}{r}\right)^{12} - \left(\frac{\sigma_B}{r}\right)^{6}\right] - \varepsilon\left[\left(\frac{\sigma_B}{r_c}\right)^{12} - \left(\frac{\sigma_B}{r_c}\right)^{6}\right] & \text{if } r \leqslant r_c \\ 0 & \text{if } r > r_c \end{cases} \tag{7.9}$$

and so

$$F_B^{trunc}(r) = \begin{cases} \left(6\frac{\varepsilon}{r}\left[2\left(\frac{\sigma_B}{r}\right)^{12} - \left(\frac{\sigma_B}{r}\right)^{6}\right] - 6\frac{\varepsilon}{r_c}\left[2\left(\frac{\sigma_B}{r_c}\right)^{12} - \left(\frac{\sigma_B}{r_c}\right)^{6}\right]\right)\vec{u}_{\vec{r}} & \text{if } r \leqslant r_c \\ \vec{0} & \text{if } r > r_c \end{cases}. \tag{7.10}$$

Interaction between two particles

In these simulations we used $\sigma_B = 1$ and so each particle has radius $R = 2^{1/6-1}$ and the cut-off distance is 2.5. We considered $\Delta t = 10^{-4}$, 10^6 iterations in time, $\varepsilon = 1$ and $L = 20$. As in model A, we want to study the difference between the passive Brownian and the active case, and so we considered two particles with initial positions $(-R,0)$ and $(R,0)$ and with initial velocity $\vec{u}_x$ and $-\vec{u}_x$, respectively.

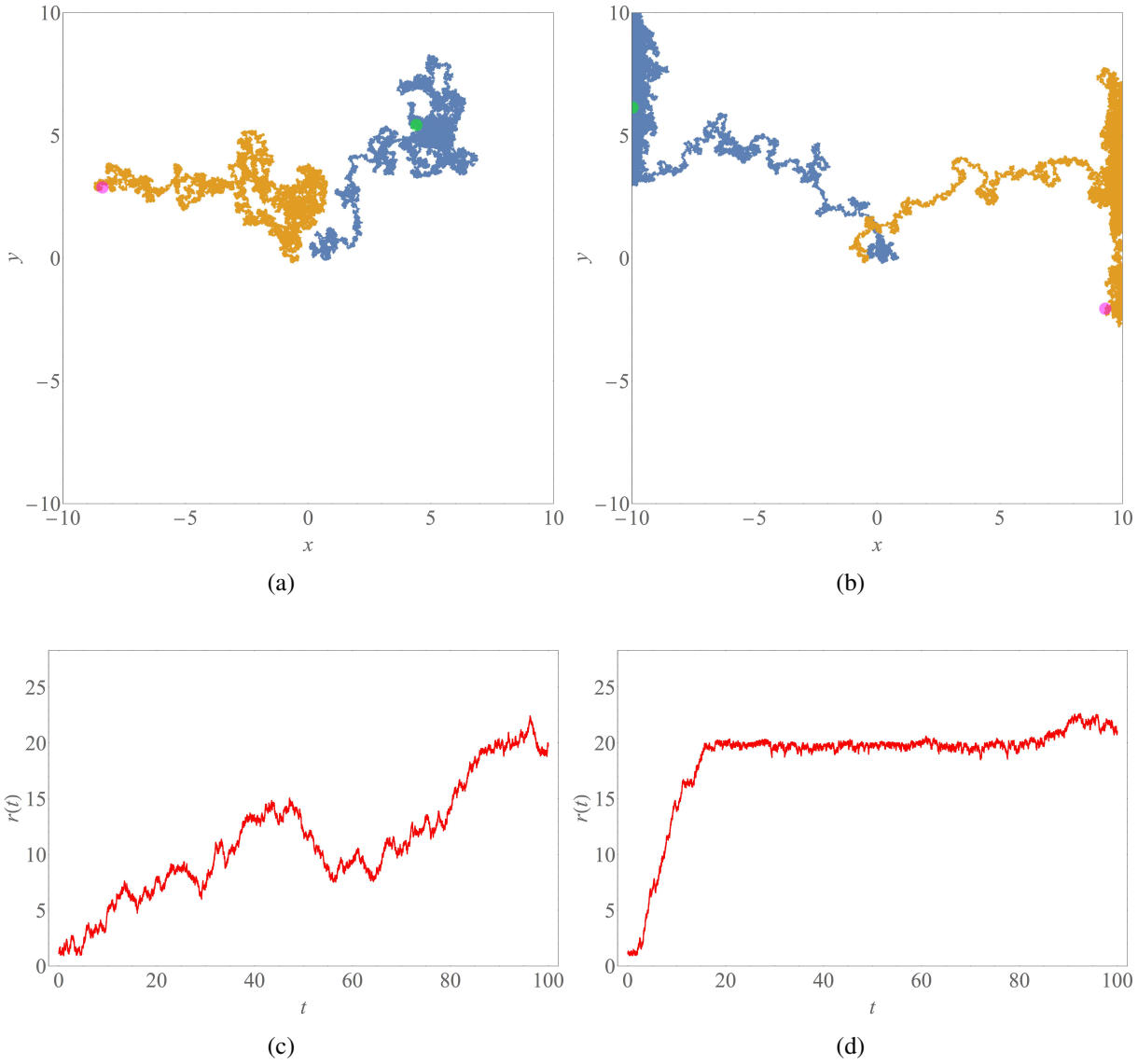

Figure 7.8: Interaction between two particles with model B when considering $\varepsilon = 1$, two passive Brownian particles (a) and (c) or two active particles with drift velocity of $v_{drift} = 1$ (b) and (d). The initial positions for the particles are $(-R,0)$ and $(R,0)$ with initial velocity $\vec{u}_x$ and $-\vec{u}_x$, respectively. In (a) and (b) it is represented the trajectory of each particle: one in orange and another in blue. The magenta and green dots represent the final position of particle in orange and blue, respectively. In (c) and (d) it is represented the distance between the two particles over time.

In this work, we are interested in studying a case with high aggregation. In order to see aggregation between two particles we searched for the *ideal* parameters where we could observe aggregation and so we studied the influence of the parameter ε in this model.

We had already seen what happens if $\varepsilon = 1$, in Figure 7.8, and here we do not see any aggregation. So let us study what happens if we consider larger or smaller values of ε.

We did simulations assuming $\Delta t = 10^{-4}$, $L = 20$ and 10^6 time steps. We considered two passive Brownian particles which were separated by a distance of $2^{1/6}$ in the start of the simulations. For the parameter ε, we consider different values in order to evaluate which one was the most suited for our future simulations. We depict the results in Figure 7.9 for $\varepsilon = 0.1$ (red line), $\varepsilon = 1$ (yellow line), $\varepsilon = 10$ (green line), $\varepsilon = 100$ (blue line) and then we also plotted the constant function $r(t) = 2^{1/6}$ (dotted magenta line). This last line was plotted because we wanted to compare the obtained results (with each value of ε) with this line. We want to find the value of ε whereby the distance between the particles is the most similar to the dotted magenta line.

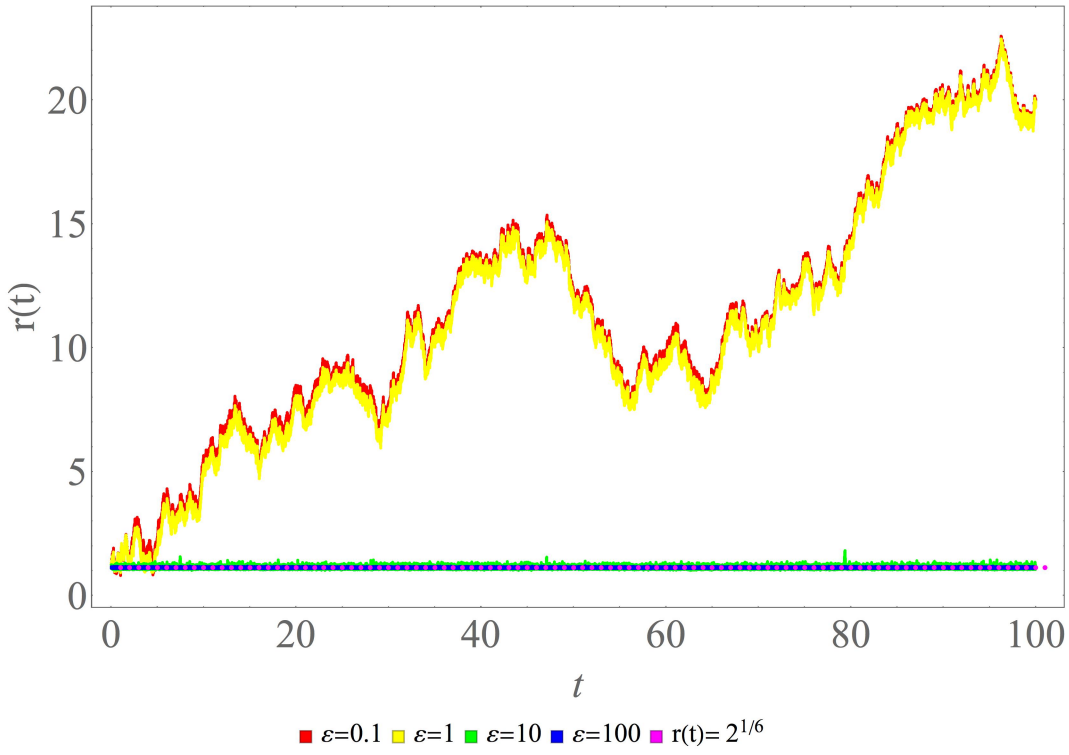

Figure 7.9: Distance between two particles for different values of ε. The dotted magenta line represents $r(t) = 2^{1/6}$.

Observing Figure 7.9, a zoomed in version of the previous figure, we see that for $\varepsilon = 0.1$ and $\varepsilon = 1$ the distance between the particles is not stable. They start to move away from each other over time, while for $\varepsilon = 10$ and $\varepsilon = 100$ we observe this distance is reasonably stable. So which value should we use between $\varepsilon = 10$ and $\varepsilon = 100$ and why?

If we zoom into the previous figure we observe

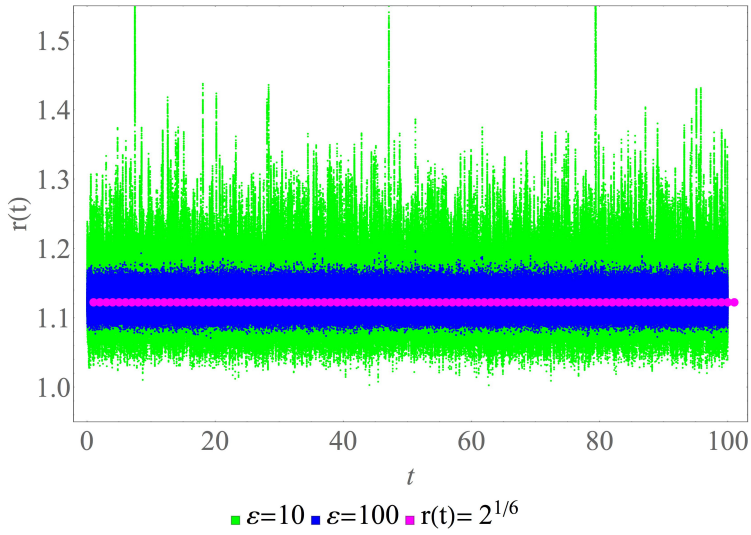

Figure 7.10: Distance between two particles for different values of ε now just for $\varepsilon = 10$ and $\varepsilon = 100$. The dotted magenta line represents $r(t) = 2^{1/6}$.

Observing Figure 7.10, which is a zoom from the previous figure, we compare these last two cases and observe that the green line, *i.e.* when $\varepsilon = 10$, shows more fluctuations of the particles distance when compared with the blue line, *i.e.* $\varepsilon = 100$. This blue line shows a more stable distance between particles, when compared with the dotted magenta line.

So we will use $\varepsilon = 100$ in our future simulations.

We performed simulations considering, again, $\sigma_B = 1$, particle radius $R = 2^{1/6-1}$, cut-off distance is 2.5, $\Delta t = 10^{-4}$, 10^6 iterations in time and $L = 20$, but now we considered $\varepsilon = 100$. As in the previous simulations, we are interested in observing the difference between the passive Brownian and the active case, and so we considered two particles with initial positions $(-R,0)$ and $(R,0)$ and with initial velocity $\vec{u}_x$ and $-\vec{u}_x$, respectively. We did simulations with passive Brownian particles, represented in Figures 7.11a and 7.11c, and with active particles (considering $v_{drift} = 1$), represented in Figures 7.11b and 7.11d.

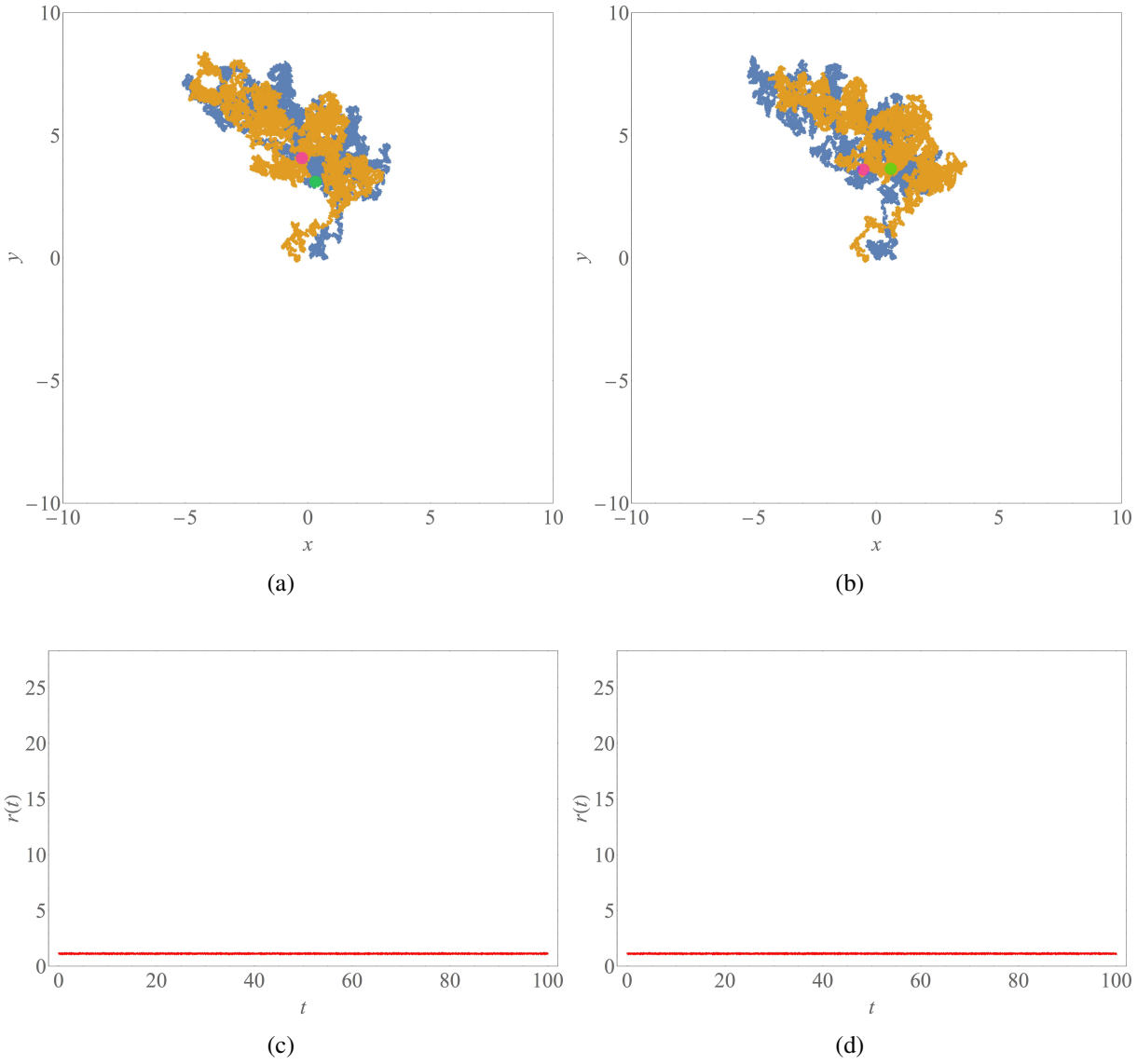

Figure 7.11: Interaction between two particles with model B when considering $\varepsilon = 100$ and two passive Brownian particles, (a) and (c), or two active particles with drift velocity of $v_{drift} = 1$, (b) and (d). The initial positions for the particles are $(-R,0)$ and $(R,0)$ with initial velocity $\vec{u}_x$ and $-\vec{u}_x$, respectively. In (a) and (b) the trajectory of each particle is represented: one in orange and another in blue. The magenta and green dots represent the final positions of the orange and blue particles respectively. In (c) and (d) the distance between the two particles over time is represented.

In Figures 7.11a and 7.11b we see the trajectory of the two particles which have initial positions $(-R,0)$ and $(R,0)$ and final positions represented by the magenta and green dot respectively. We can see that in both of these figures the particles have similar trajectories. Even if in these figures we cannot visually affirm that aggregation occurred, by Figures 7.11c and 7.11d we can see that distance between the particles is constant over time and so the particles aggregated, as expected.

Interaction between several particles

After studying the case with two particles, we moved on to the study of a case with several particles in which, again, we are interested in studying the probability density function of this model when we consider different values of v_{drift}. Our simulations were performed with $L = 20$, $\varepsilon = 100$, $\sigma_B = 1$, 10^2 particles, 10^3 samples, $\Delta t = 10^{-4}$, $D_T = 0.2$ and different total simulation times.

The first case studied was the passive Brownian case. In Figure 7.12 we can see the probability density function for simulations considering passive Brownian particles and different values of total simulation time. In this figure, we see that the probability density function converges to a uniform distribution as was observed in model A. Again, we can notice some fluctuations which are due to the number of samples.

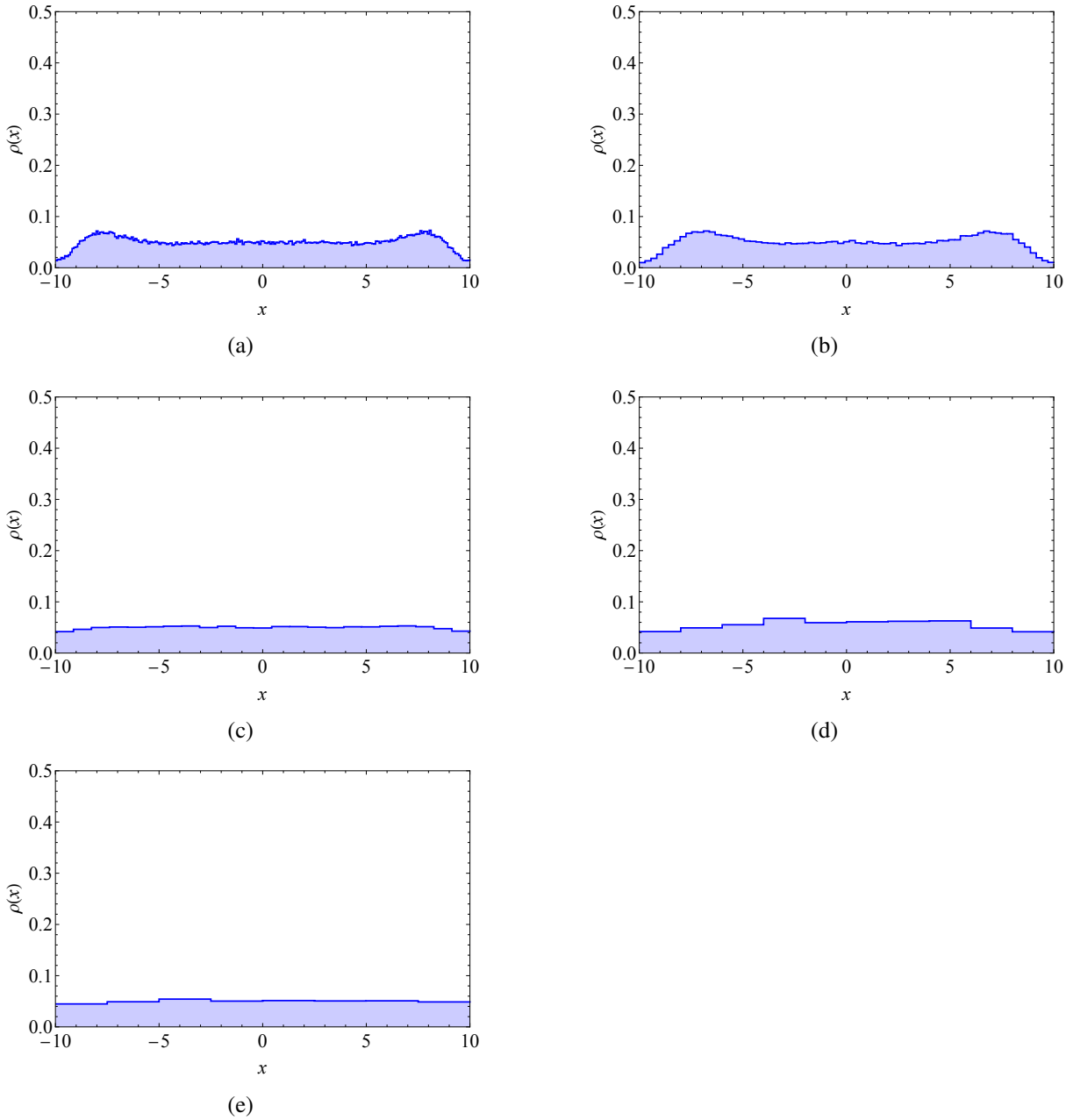

Figure 7.12: Probability density function considering passive Brownian particles. The total simulation time for (a), (b), (c), (d) and (e) is, respectively, 1, 10, 10^2, 5×10^2 and 10^3.

Then we studied an active case in which the particles had active particles with drift velocity of $v_{drift} = 1$. Again, these simulations were performed considering $L = 20$, $\varepsilon = 100$, $\sigma_B = 1$, 10^2 particles, 10^3 samples, $\Delta t = 10^{-4}$, $D_T = 0.2$ and different total simulation time: 1, 10, 10^2, 5×10^2 and 10^3.

We can observe that the probability density function increases close to the walls and decreases in the bulk over time by observing Figure 7.13. For a total simulation time 10^3, in Figure 7.13e, we can see clearly see accumulation of particles close to the walls. This was observed in model A when we considered the active case with $v_{drift} = 1$, and we also observed that this process, accumulation of particles near the walls, occurs faster in model B than in model A.

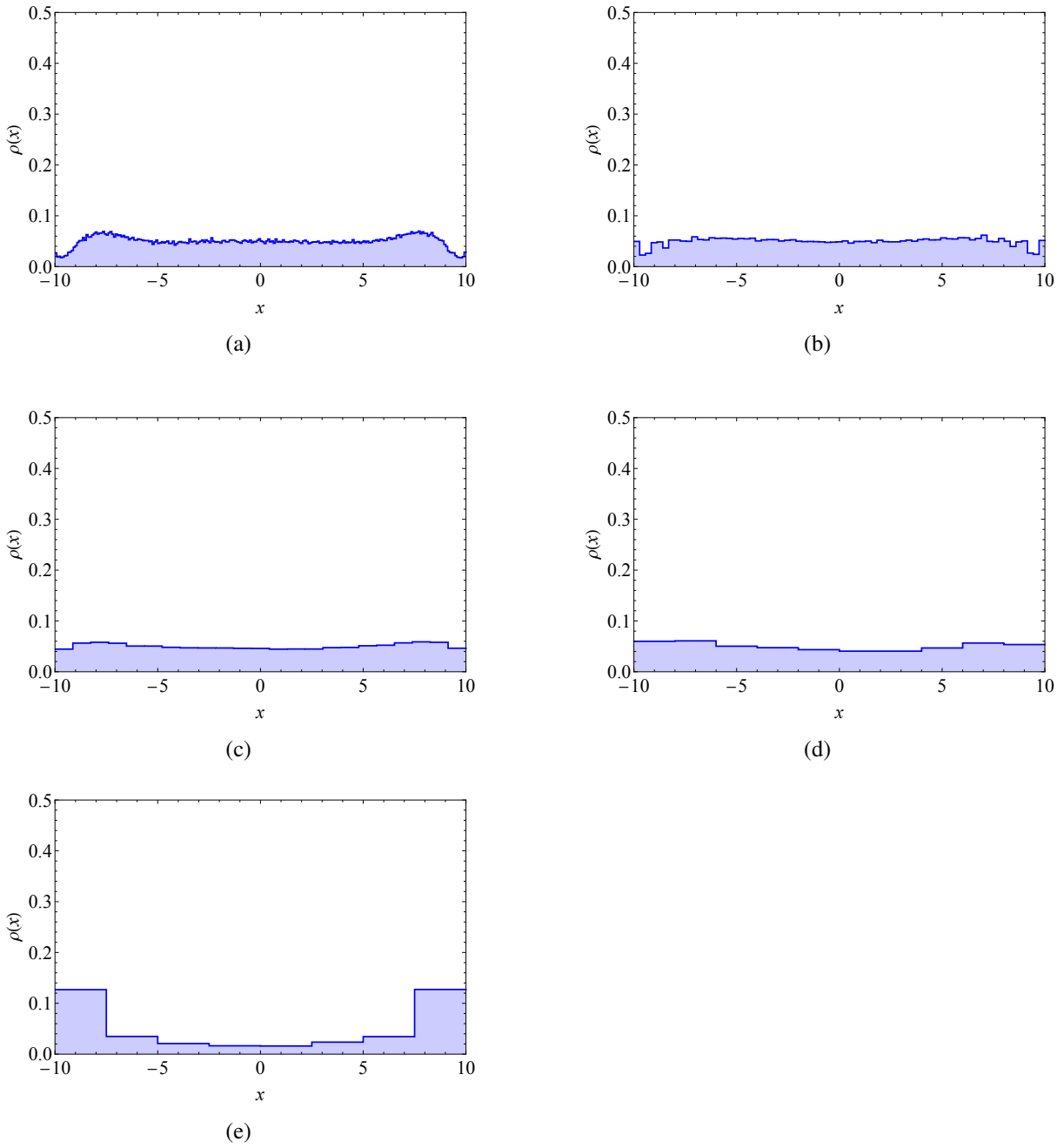

Figure 7.13: Probability density function considering active particles with $v_{drift} = 1$. The total simulation time for (a), (b), (c), (d) and (e) is, respectively, 1, 10, 10^2, 5×10^2 and 10^3.

Then we considered another active case but now with a larger drift velocity, $v_{drift} = 5$, so that we can compare with the previous case when $v_{drift} = 1$. Here we considered, again, $L = 20$, $\varepsilon = 100$, $\sigma_B = 1$, 10^2 particles, 10^3 samples, $\Delta t = 10^{-4}$, $D_T = 0.2$ and different total simulation times: 1, 10, 10^2, 5×10^2 and 10^3.

As in the previous case, where $v_{drift} = 1$, we can observe in Figure 7.14 that the particles start to accumulate near the walls over time. As the time increases, we can see that probability density function converges to zero in the bulk area and that the maximum value of this function increases near the walls.

If we compare Figure 7.14 with Figure 7.13 we see that the accumulation of particles near the walls is faster when we consider $v_{drift} = 5$ than $v_{drift} = 1$.

Now, if we compare this model with model A in the case in which $v_{drift} = 5$, we see, again, that the accumulation near the walls occurs faster in model A than in model B.

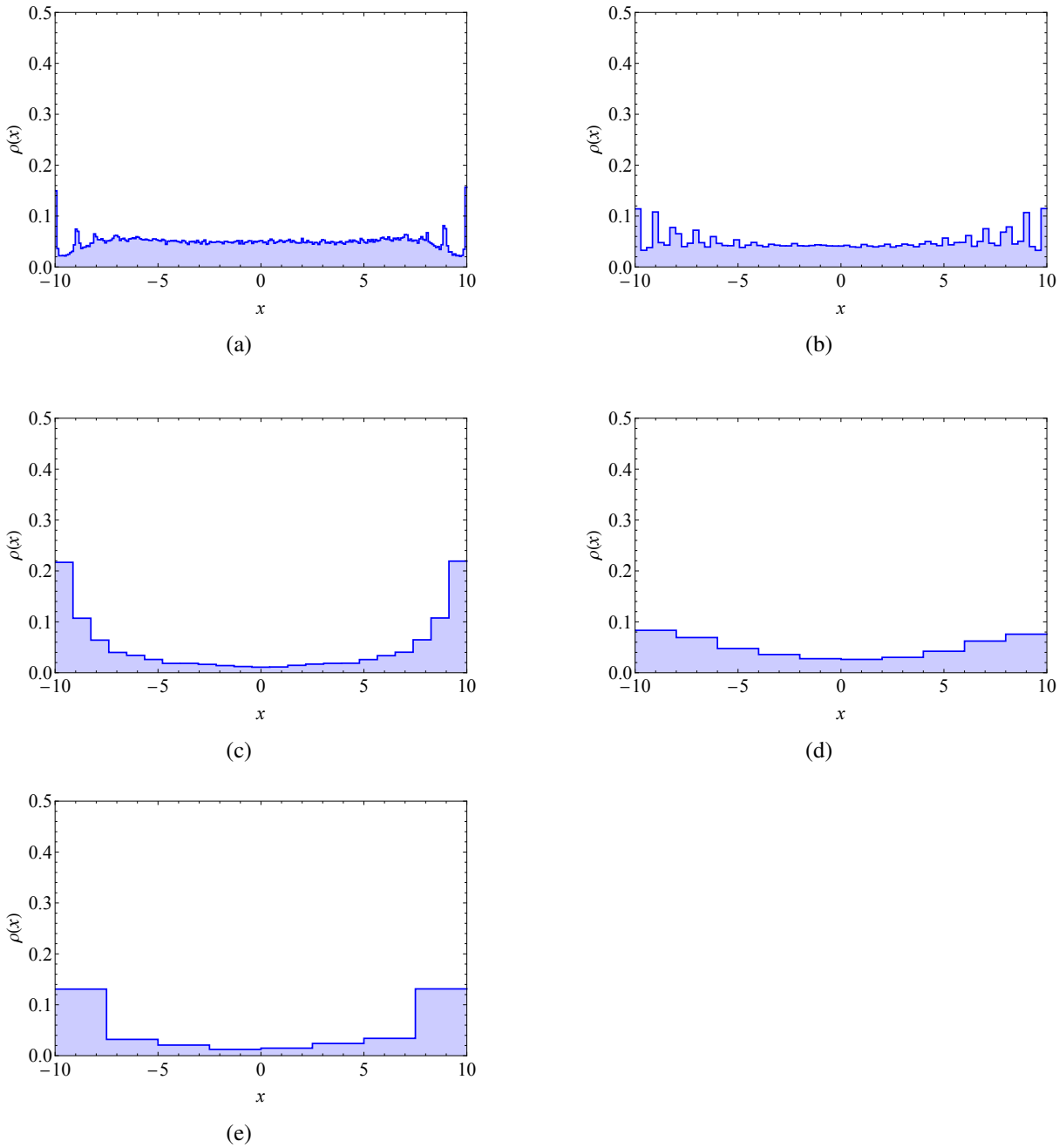

Figure 7.14: Probability density function of particles with $v_{drift} = 5$. The total simulation time for (a), (b), (c), (d) and (e) is, respectively, 1, 10, 10^2, 5×10^2 and 10^3.

Chapter 8

Conclusion

In this work, we have discussed coupled Wiener processes and how we can use them to describe the motion of active and passive Brownian particles mathematically. The motion of active particles being of most interest to us, as a better mathematical understanding of these motions sets the groundwork for many modern-day applications such as the micro- and nano-robots briefly discussed in our introduction.

In our work we focussed on a two-dimensional system with circular shaped particles. After the preliminary work of discussing all the equations and deductions that our simulations are based upon we ran multiple series of numerical simulations, the observations of which we will now describe in brief and the related conclusions.

When simulating a system in which we considered periodic boundary conditions, we observed that passive Brownian particles have a purely diffusive behaviour over time, whereas in the active particle case, diffusive behaviour is observed when the time is much larger than the inverse of the rotational diffusion coefficient, but for times smaller than this the behaviour of these particles is ballistic.

For the rest of the simulations we introduced the presence of a square boundary wall. We observed that the probability density function of passive Brownian particles that started in square centre converges over time from a normal distribution to a uniform distribution with no accumulation of particles near the wall. Active particles on the other hand displayed a probability density function that over time had increased values near the walls and decreased values in the bulk. When keeping time fixed and varying the drift velocity of the active particles, the same observation was made. We can conclude that in the presence of a boundary active particles will start to accumulate near this boundary, the speed of which depends on the time and/or their drift velocity. This result can be explained as follows. From theory we know that when an active particle interacts with a wall, there is an asymmetry between the motion of approach and leave the wall. When the particle approaches the wall, it will stay close to the wall until its orientation points away from it and when the particle leaves the wall it will swim away. Such an asymmetry of motion gives us a tendency of accumulation of active particles near walls. In numerical simulation terms, the simulation must make quite some iterations before the random number generator that gives us the rotational change gives a new random number so that the new angle is considerably different from the previous one.

This is important in active particle applications such as drug delivery to specific locations of the body via micro- and nano-robots as these particles (robots) will tend to accumulate near boundary surfaces in the body leading to higher doses of drugs in either desirable or undesirable locations which can result in side effects. As we showed in our simulations, by varying the particle's drift velocity or the drug release time period this accumulation effect could be (partially) controlled. We expanded our simulation series by studying the influence of varying the translational diffusion coefficient (and so the rotational diffu-

sion coefficient). We found that a dependency exists between the translational diffusion coefficient and total simulation time and also between the translational diffusion coefficient and the particle drift velocity. Our baseline simulation of passive Brownian particles showed us that with a fixed time, increasing the translational diffusion coefficient gave us an increasingly wider probability density function curve (closer to a uniform distribution). Also, over time for all the translational diffusion coefficients studied the probability density function became wider (closer to a uniform distribution) as was already observed in the simulations with the original fixed translational diffusion coefficient. When looking at the case of active particles with varying translational diffusion coefficient we observed the same differences in behaviour from passive Brownian particles as in the simulations introducing a square boundary: when we increase the drift velocity in the four different translational diffusion coefficients we observe a faster particle accumulation near the boundaries. Also, with a fixed drift velocity, over time the probability density function values near the boundaries became larger, i.e. higher particle accumulation near the walls, with all four translational diffusion coefficients. What is interesting is that once particle accumulation near the wall occurs, the boundary values in the probability density function are larger for smaller translational diffusion coefficient mediums. What is happening is that even though some active particles in larger translational diffusion coefficient mediums reach the boundary quicker, due to the larger translational diffusion coefficient (and therefore also larger rotational diffusion coefficient), these particles can also periodically leave the boundary further (smaller translational diffusion coefficient) and more often (larger rotational diffusion coefficient) leading to less of a narrow peak in the probability density function at the boundary. Again, this effect has implications for practical implications such as the before mentioned drug distribution within the body, as blood (having a smaller translational diffusion coefficient) will lead to a denser accumulation of particles near boundaries.

To stay with our example of micro- and nano-robots, practical application will often imply using a large number of individual robots and these particles will cause interactions with each other which need to be understood. So, to end our simulation series we studied particle-particle interaction. We studied two different potential models: the repulsive potential and the Lennard-Jones potential. With two passive Brownian particles tangent to each other, both potential models display the particles repelling and moving away from each other. The same happens with two active particles although, after a certain time the distance between the stays approximately stable. With several particles in the system the same behaviour regarding the probability density function occurs in the simulations as when no potential was modelled in earlier simulations: the probability density function of passive Brownian particles converges to a uniform distribution and with active particles, the probability density function shows higher values towards the boundaries over time, which again, occurs faster with larger values of drift velocity. There are differences between the potential models though: passive Brownian particles take longer to uniformly distribute when using the repulsive potential model and thus for the probability density function to converge to a uniform distribution. For active particles, accumulation near the wall occurs faster when using a repulsive potential than when using the Lennard-Jones potential, which is expected when thinking in physical terms. With active particles using the Lennard-Jones potential, when $\varepsilon \to 0$ the attraction between the particles is weaker and so this converges to a non-aggregation state. But when $\varepsilon \gg 1$ there is a strong aggregation and this is independent of drift velocity.

As future research topics, we can think about the challenge of having obstacles in the medium [1]. E.g. it would be interesting to study the influence of the geometry of the obstacle in the accumulation of particles. Another interesting study would be the chiral active motion in which active particles swim in circles trajectories [1]. More knowledge on these topics will allow us to exert more control over active particles and, in particular, man-made active particles such as aforementioned micro- and nano-robots.

Bibliography

[1] C. Bechinger *et al*. *Active particles in complex and crowded environments*. Review Modern Physics **Vol. 88 Issue 4** 045006-045056 (2016).

[2] K. Drescher *et al*. *Fluid dynamics and noise in bacterial cell-cell and cell-surface scattering*. PNAS **27** 10940 – 10945 (2011).

[3] P. Góra. *The theory of Brownian Motion: A Hundred Years' Anniversary*. Foton **Special issue** 52 – 57 (2006).

[4] G. Zhao *et al*. *Poisoning of bubble propelled catalytic micromotors: the chemical environment matters*. Nanoscale **5** 2909 (2013).

[5] F. Knäble. *Ornstein-Uhlenbeck Equations with time-dependent coefficients and Lévy Noise in finite and infinite dimensions*. Journal of Evolution Equations, **Vol. 11 No. 4**, 959-993 (2011).

[6] A. Widiatmojo, K. Sasaki, N. Priagung Widodo and Y. Sugai *Discrete Tracer Point Method to Evaluate Turbulent Diffusion in Circular Pipe Flow*. Journal of Flow Control, Measurement & Visualization **Vol. 1 No. 2** 57-68 (2013).

[7] B. Øksendal. *Stochastic Differential Equations: An Introduction with Applications*. US: Springer (1998).

[8] P. E. Kloeden and E. Platen. *Numerical Solution of Stochastic Differential Equations*. Berlin: Springer-Verlag (1992).

[9] S. M. Iacus *Simulation and Inference for Stochastic Differential Equations*. Springer (2008).

[10] C. W. Gardiner. *Handbook of Stochastic Methods for Physics, Chemistry and the Natural Sciences*. US: Springer (1985).

[11] P. Krapivsky, S. Redner, E. Ben-Naim. *A Kinetic view of Statistical Physics*. US: Cambridge University Press (2010).

[12] F. Reif. *Fundamentals of Statistical and Thermal Physics*. US: McGraw-Hill (2009).

[13] D. Knuth *The Art of Computer Programming, Volume 1*. Addison-Wesley (1968).

[14] R. Landau, M. Páez and C. Bordeianu. *A Survey of Computational Physics*. Princeton University Press (2010).

[15] L. Arnold. *Stochastic Differential Equations: Theory and Applications*. John Wiley and Sons (1974).

Appendix

A The formal derivative and white noise

Fix a ring R (not necessarily commutative) and let $A = R[x]$ be the ring of polynomials over R. Then the **formal derivative** is an operation on elements over A, where if $p(x) = a_n x^n + ... + a_1 x + a_0$ then its formal derivative is given by

$$\frac{dp(x)}{dx} = na_n x^{n-1} + ... + 2a_2 x + a_1. \tag{1}$$

Note that here na_n does not mean multiplication in the ring, but rather $\sum_{k=1}^{n} a_k$.

The algebraic advantage of this derivative is that it does not rely on the notation of a limit, which is, in general, impossible to define for a ring.

Now let us use the concept of formal derivative to define white noise.

Suppose a Wiener process $W(t)$. Since this process has probability 1 of being non-differentiable then the white noise defined in Definition 2.3 can be also defined as the formal derivative of a Wiener process and it is written as

$$\xi(t) := \frac{dW(t)}{dt}. \tag{2}$$

B Units of simulation

Let us define u_L and u_T as the simulation units of length and time, respectively.

In this work we considered micro- and nano-particles, *i.e.*, particles with an average size between 10^{-6} m and 10^{-9} m. To perform our simulations, we considered spherical particles of real diameter of 10^{-6} m and so we defined u_L such that 1 $u_L = 10^{-6}$ m. Then we considered 1 s = 1 u_T to define the simulation unit of time.

We used these units of simulation in every value that we considered in this work.

C Software and hardware

In this work we used the following software and hardware resources:

- for the **simulations**:
  1. *Xcode*, Version 8.0 beta 5, Language: *C++*;
  2. *High Performance Computing* from Centro de Física Teórica e Computacional (CFTC) of Faculdade de Ciências da Universidade de Lisboa: 180 Gb of RAM, 1 Gb/s of Gigabit network, 168 cores, 21 nodes - 8 cores of 2.5GHz;

- for the **data plots**:
  1. *Grace*, Version 5.1.22;
  2. *Wolfram Mathematica*, Version 11.01.0.